Journal of Medicinal Chemistry

Article

FimH Antagonists - Bioisosteres to Improve the PK/PD Profile

Beat Ernst, Simon - Kleeb, Lijuan Pang, Katharina Mayer, Deniz Eris, Anja Sigl, Pacal Zihlmann, Roland Christopher Preston, Timothy Sharpe, Roman Jakob, Daniela Abgottspon, Aline S. Hutter, Meike Scharenberg, Xiaohua Jiang, Giulio Navarra, Said Rabbani, Martin Smiesko, Nathalie Lüdin, Jacqueline Bezencon, Oliver Schwardt, and Timm Maier

J. Med. Chem., **Just Accepted Manuscript** • Publication Date (Web): 10 Feb 2015

Just Accepted

Journal of Medicinal Chemistry is published by the American Chemical Society.
1155 Sixteenth Street N.W., Washington, DC 20036

FimH Antagonists - Bioisosteres to Improve the *in vitro* and *in vivo* PK/PD Profile

Simon Kleeb,[a)]# Lijuan Pang,[a)]# Katharina Mayer,[a)]# Deniz Eris,[a)]# Anja Sigl,[a)]# Roland C. Preston,[a)] Pascal Zihlmann,[a)] Timothy Sharpe,[c)] Roman P. Jakob,[b)] Daniela Abgottspon,[a)] Aline S. Hutter,[a)] Meike Scharenberg,[a)] Xiaohua Jiang,[a)] Giulio Navarra,[a)] Said Rabbani,[a)] Martin Smiesko,[a)] Nathalie Lüdin,[a)] Jacqueline Bezençon,[a)] Oliver Schwardt,[a)] Timm Maier,[b)] Beat Ernst [a)]*

# Equally contributed

[a)] Institute of Molecular Pharmacy, Pharmacenter, University of Basel, Klingelbergstrasse 50, CH-4056 Basel, Switzerland

[b)] Structural Biology, Biocenter, University of Basel, Klingelbergstrasse 70, CH-4056 Basel

[c)] Biophysical Facility, Biocenter, University of Basel, Klingelbergstrasse 70, CH-4056 Basel

* To whom correspondence should be addressed: Prof. Dr. Beat Ernst, Institute of Molecular Pharmacy, Pharmacenter, University of Basel, Klingelbergstrasse 50, CH-4056 Basel, Switzerland; Tel: +41 61 267 15 51, Fax: +41 61 267 15 52; E-mail: beat.ernst@unibas.ch

ABBREVIATIONS:

ΔH, change in enthalpy; ΔS, change in entropy; AUC, Area under the curve; BSA, bovine serum albumin; C_{max}, maximal concentration; Caco-2 cells, colorectal adenocarcinoma cells; CFU, colony forming units; CL_{tot}, total clearance; CRD, carbohydrate recognition domain; C_0, initial concentration; DL: detection limit; FITC, fluorescein isothiocyanate; FP, fluorescence polarization; ITC, isothermal titration calorimetry; i.v., intravenous; K_D, dissociation constant; MAC_{90}, minimal anti-adhesion concentration to inhibit 90% adhesion; PAMPA, parallel artificial membrane permeation assay; P_{app}, apparent permeability; PD, pharmacodynamics; P_e, effective permeability; PK, pharmacokinetics; p.o., per os; s.c. subcutaneous; UPEC,

uropathogenic *Escherichia coli*; UTI, urinary tract infection; V_z, volume of distribution in terminal phase.

ABSTRACT

Urinary tract infections (UTIs), predominantly caused by uropathogenic *Escherichia coli* (UPEC) belong to the most prevalent infectious diseases worldwide. The attachment of UPEC to host cells is mediated by FimH, a mannose-binding adhesin at the tip of bacterial type 1 pili. To date, UTIs are mainly treated with antibiotics, leading to the ubiquitous problem of increasing resistance against most of the currently available antimicrobials. Therefore, new treatment strategies are urgently needed. Here, we describe the development of an orally available FimH antagonist. Starting from the carboxylate substituted biphenyl α-D-mannoside **9** affinity as well as the relevant pharmacokinetic parameters (solubility, permeability, renal excretion) were substantially improved by a bioisosteric approach. With 3'-chloro-4'-(α-D-mannopyranosyloxy)-biphenyl-4-carbonitrile (**10j**) a FimH antagonist with an optimal *in vitro* PK/PD profile was identified. Orally applied, **10j** was effective in a mouse model of UTI by reducing the bacterial load in the bladder by about 1000-fold.

INTRODUCTION

Urinary tract infection (UTI) is one of the most frequent infectious diseases worldwide and affects millions of people every year.[1] In more than 70% of the reported cases, uropathogenic *Escherichia coli* (UPEC) is the causal pathogen.[2] Acute, uncomplicated lower urinary tract infection, commonly referred to as cystitis, requires an antibiotic treatment for symptom relief (i.e. reduction of dysuria, frequent and urgent urination, bacteriuria, pyuria) and for prevention of more devastating or even life threatening complications like pyelonephritis and urosepsis.[3,4] However, the repeated use of antibacterial chemotherapeutics provokes antimicrobial resistance leading to treatment failure.[5] Hence, a new approach for the prevention and treatment of UTI with orally applicable therapeutics is urgently needed.[6]

UPEC undergo a well-defined infection cycle within the host.[7] The key step in pathogenesis is bacterial adhesion to the epithelial cells in the lower urinary tract.[8] This interaction prevents UPEC from clearance by the bulk flow of urine and enables the bacteria to colonize the epithelial cells. The adhesion is mediated by the virulence factor FimH located at the tip of bacterial type 1 pili.[9,10] FimH consists of two immunoglobulin-like domains: the N-terminal lectin domain and – connected by a short linker – the C-terminal pilin domain.[11] The lectin domain encloses the carbohydrate recognition domain (CRD) that binds to the oligomannosides of the glycoprotein uroplakin Ia on the epithelial cell surface.[12] The pilin domain anchors the adhesin to the pilus and regulates the switch between two conformational states of the CRD with high and low affinity for mannosides, respectively.

More than three decades ago, Sharon and co-workers described various oligomannosides and aryl α-D-mannosides as potential antagonists of the FimH-mediated bacterial adhesion.[13,14]

However, only weak interactions in the milli- to micromolar range were observed. In recent years, several high-affinity monovalent mannose-based FimH antagonists with various aglycones like *n*-alkyl,[15] phenyl,[16] dioxocyclobutenylaminophenyl,[17] umbelliferyl,[16] biphenyl,[18-22] indol(in)ylphenyl,[23] triazolyl[24] and thiazolylamino[25] have been reported. In addition, different multivalent presentations of the mannose have been synthesized[26-32] and a heptavalent presentation of *n*-heptyl α-D-mannoside (**1**) tethered to β-cyclodextin proved to be highly effective when applied together with the UTI89 bacterial strain through a catheter into the bladder of C3H/HeN mice.[32] Importantly, adverse side effects resulting from non-selective binding of FimH antagonists - they are all α-D-mannopyranosides - to mannose receptors of the human host system have recently been ruled out.[33]

The high affinities of the monovalent α-D-mannopyranosides are based on optimal interactions with the main structural features of the CRD.[34-37] First, the mannose binding pocket accommodating the mannose moiety by means of an extended hydrogen bond network and, second, the entrance to the binding site composed of three hydrophobic amino acids (Tyr48, Tyr137, and Ile52) and therefore referred to as 'tyrosine gate' hosting aliphatic and aromatic aglycones. As an example, *n*-heptyl α-D-mannopyranoside (**1**) exhibits nanomolar affinity due to hydrophobic contacts of the alkyl aglycone with the hydrophobic residues of the tyrosine gate.[15] Furthermore, aromatic aglycones, such as present in mannosides **2** & **3** (Figure 1), provide strong π-π stacking interactions with the tyrosine gate. This interaction is further favored by the addition of an electron withdrawing substituent on the terminal ring of the biaryl portion (→ **4**).[18,19]

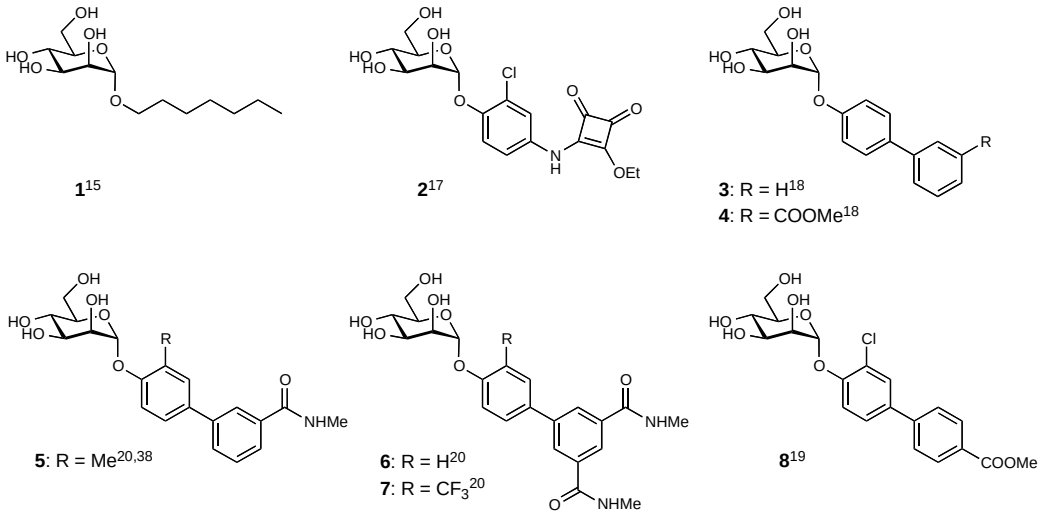

Figure 1. Monovalent FimH antagonists **1**-**4** acting as reference compounds and **5**-**8** which have been orally explored in *in vivo* disease models.

Recent *in vivo* PK studies in mice proved the high potential of the biphenyl α-D-mannosides **5**-**8** for an oral treatment, although high doses (≥ 50 mg/kg) were necessary to achieve the minimal concentrations required for the anti-adhesive effect in the urinary bladder.[19-21] Moreover, the therapeutic effect could only be maintained for a few hours, i.e. four hours for a p.o. (per os) single-dose application of **7** (50 mg/kg), because of rapid elimination by glomerular filtration and low reabsorption from the primary urine in the renal tubules.[19]

To date, the physicochemical properties affecting the rate of renal excretion, i.e. lipophilicity and plasma protein binding (PPB), or metabolic liabilities promoting non-renal elimination pathways have been barely investigated for FimH antagonists. The goal of the present study was to optimize the biphenyl α-D-mannoside with respect to oral bioavailability and renal excretion. Starting from antagonist **9**[19] (Figure 2), we synthesized new biphenyl derivatives, characterized their affinity to the CRD, structurally investigated their binding mode, and determined physicochemical and pharmacokinetic parameters predictive for intestinal

absorption and renal elimination. Furthermore, we determined *in vivo* PK (pharmacokinetics) of the most promising new antagonists in a mouse model. After oral administration, the compound with the best PK profile proofed effective in reducing the bacterial loads upon bladder infection in a mouse model of UTI.

RESULTS AND DISCUSSION

As previously reported, the carboxylate substituent present in the biphenyl mannoside **9** – its electron withdrawing potential being essential for an enhanced drug target interaction – strongly decreases the lipophilicity of the antagonist (log $D_{7.4}$ < -1.5[19]) in comparison to the *n*-heptyl (→ **1**, log *P* = 1.7[19]) or the unsubstituted biphenyl aglycone (→ **3**, log *P* = 2.1[22]). Since low lipophilicity is a major reason for low intestinal absorption and rapid renal excretion of the systemically available antagonist,[19,23] we aspired to improve oral bioavailability as well as renal excretion by replacing the carboxylate in **9** with various bioisosteric groups[39] (Figure 2).

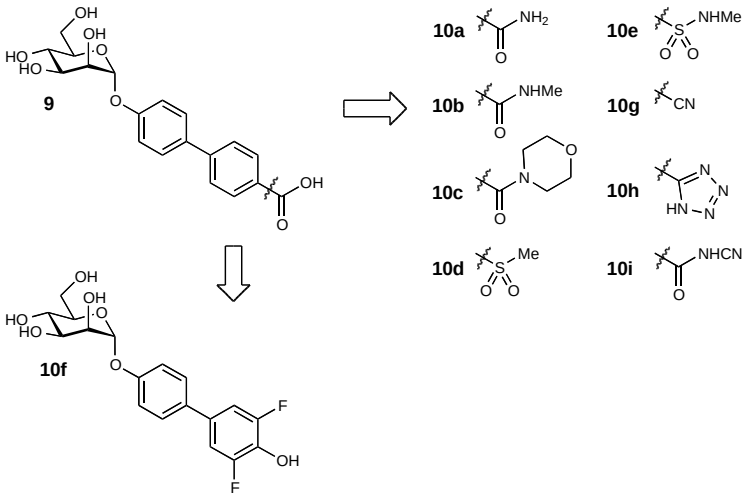

Figure 2. Bioisosteric replacement of the carboxylic acid substituent of biphenyl α-D-mannopyranoside **9**.

Synthesis. Iodide **11** was prepared from peracetylated mannose and 4-iodophenol in the presence of $BF_3 \cdot Et_2O$.[22] In a palladium-catalyzed Miyaura-Suzuki coupling[40] with the boronic acid or boronate derivatives **12a-g**, the biphenyl derivatives **13a-g** were obtained in good to excellent yields. Final deprotection yielded the test compounds **10a-g**. Utilizing microwave-assisted reaction conditions,[41] the conversion of arylnitrile **13g** to tetrazole **14** proceeded rapidly and with good yield. After deprotection of **14** using Zemplén conditions, the test compound **10h** was obtained (Scheme 1).

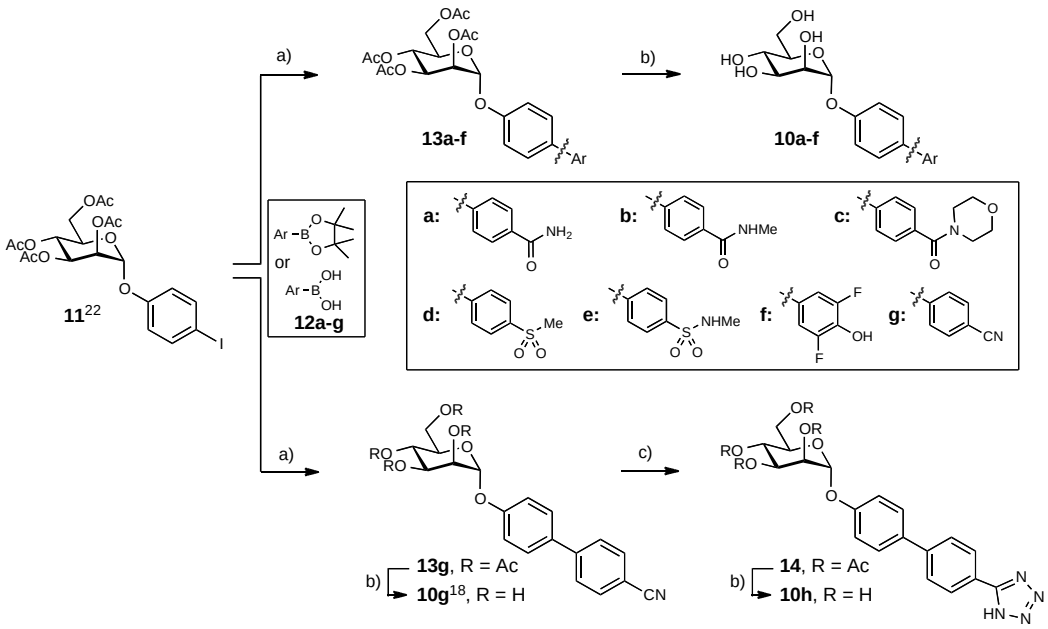

Scheme 1. a) $Pd(Cl_2)dppf \cdot CH_2Cl_2$, K_3PO_4, DMF, 80 °C, 4 h (**13a-g**, 44-99%); b) NaOMe, MeOH, rt, 4 h (**10a-h**, 29-86%); c) $TMSN_3$, $Bu_2Sn(O)$, DME, 150 °C, μW, 10 min (81%).

The cyanobenzamide derivative **10i** (Scheme 2) was obtained from **9** by peracetylation (→ **15**) followed by conversion of the carboxylic acid into its acid chloride with 1-chloro-*N*,*N*,2-trimethyl-1-propenylamine.[42] Without isolation, the acid chloride was reacted with sodium hydrogen cyanamide in DMF followed by deacetylation under Zemplén conditions to yield the test compound **10i**.

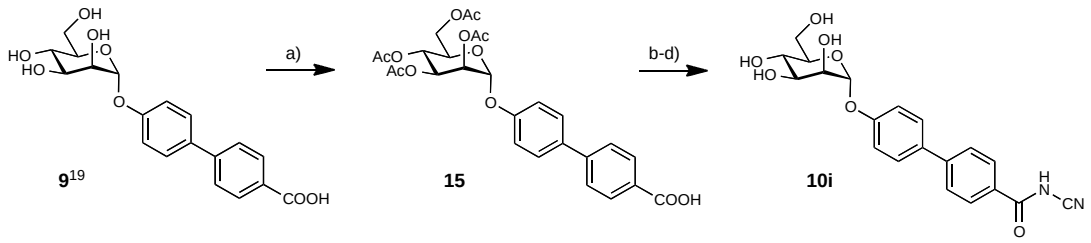

Scheme 2. a) i) Ac_2O, DMAP, pyridine, 0 °C to rt, overnight; ii) satd. $NaHCO_3$ aq., DCM, rt, 2 h (**15**, 53%); b) 1-chloro-*N*,*N*,2-trimethyl-1-propenylamine, toluene, 0 °C to rt, 2 h; c) NaH, NH_2CN, DMF, 0 °C to rt, overnight; d) NaOMe, MeOH, rt, 4 h (**10i**, 21% for three steps).

Finally, to further improve the pharmacokinetic properties of mannoside **10g**[18] (see Table 3), a chloride substituent was introduced to the *ortho*-position of the aromatic ring adjacent to the anomeric oxygen. For its synthesis, peracylated α-D-mannose (**16**) was coupled with 2-chloro-4-iodophenol (**17**) using $BF_3{\cdot}Et_2O$ as promotor (→ **18**, 76%). After the introduction of the second aromatic ring by Miyaura-Suzuki coupling (→ **19**, 75%), deprotection yielded mannoside **10j** (Scheme 3).

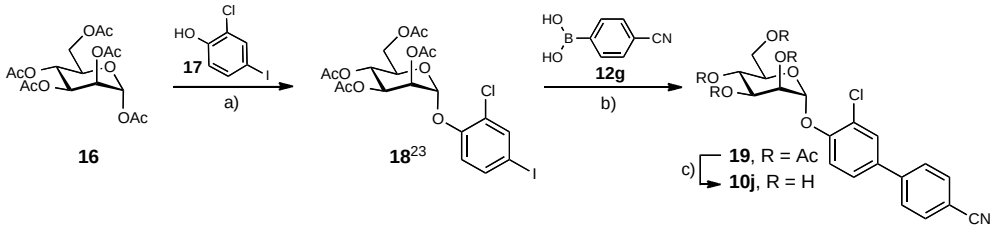

Scheme 3. a) $BF_3{\cdot}Et_2O$, CH_2Cl_2, 40 °C (76%); b) $Pd(Cl_2)dppf{\cdot}CH_2Cl_2$, K_3PO_4, DMF, 80 °C (75%); c) NaOMe, MeOH, rt, 4 h (48%).

Binding Affinity. The binding affinity of heptyl mannoside **1**, the biphenyl mannosides **3**, **9**, **20**,[18] and the bioisosteres **10a-j** was determined in a competitive fluorescence polarization assay (FP-assay) and with isothermal titration calorimetry (ITC). A protein construct consisting of the CRD with a C-terminal His-tag with a thrombin cleavage site (FimH-CRD-Th-His_6) was used for all experiments.[43]

Competitive Fluorescence Polarization Assay. For the rapid evaluation of binding affinity, we established a competitive binding assay based on fluorescence polarization (FP). Similar formats have been applied before for the detection of carbohydrate-lectin interactions.[18,44] In this assay, the antagonist of interest displaces a fluorescently labeled competitor from the binding site, thereby causing a reduction in fluorescence polarization.[45] To identify the optimal competitor, fluorescein isothiocyanate (FITC) was connected to the FimH ligand **21** by three linkers of different lengths (→ **22**-**24**, Scheme 4). For optimal sensitivity and signal-to-noise ratio, three main parameters need to be considered: (i) the affinity of the competitor should not be impaired by the fluorescent label, (ii) the conformational flexibility of the label upon binding of the competitor to the CRD should be low and (iii) the fluorescence properties of the label should not be affected by the connected ligand.[46-48] A change in fluorescence properties was observed for reporter ligand **22** in which the label was linked to the biphenyl agylcone by an amide bond. The absorption spectrum revealed a lack of the characteristic fluorescein absorption peak at 494 nm (Scheme 4), likely due to an extension of the conjugated system to the biphenyl moiety of the ligand. The elongated saturated spacer groups in competitors **23** and **24** ensured that the expected spectral properties of the dye were retained (Scheme 4).

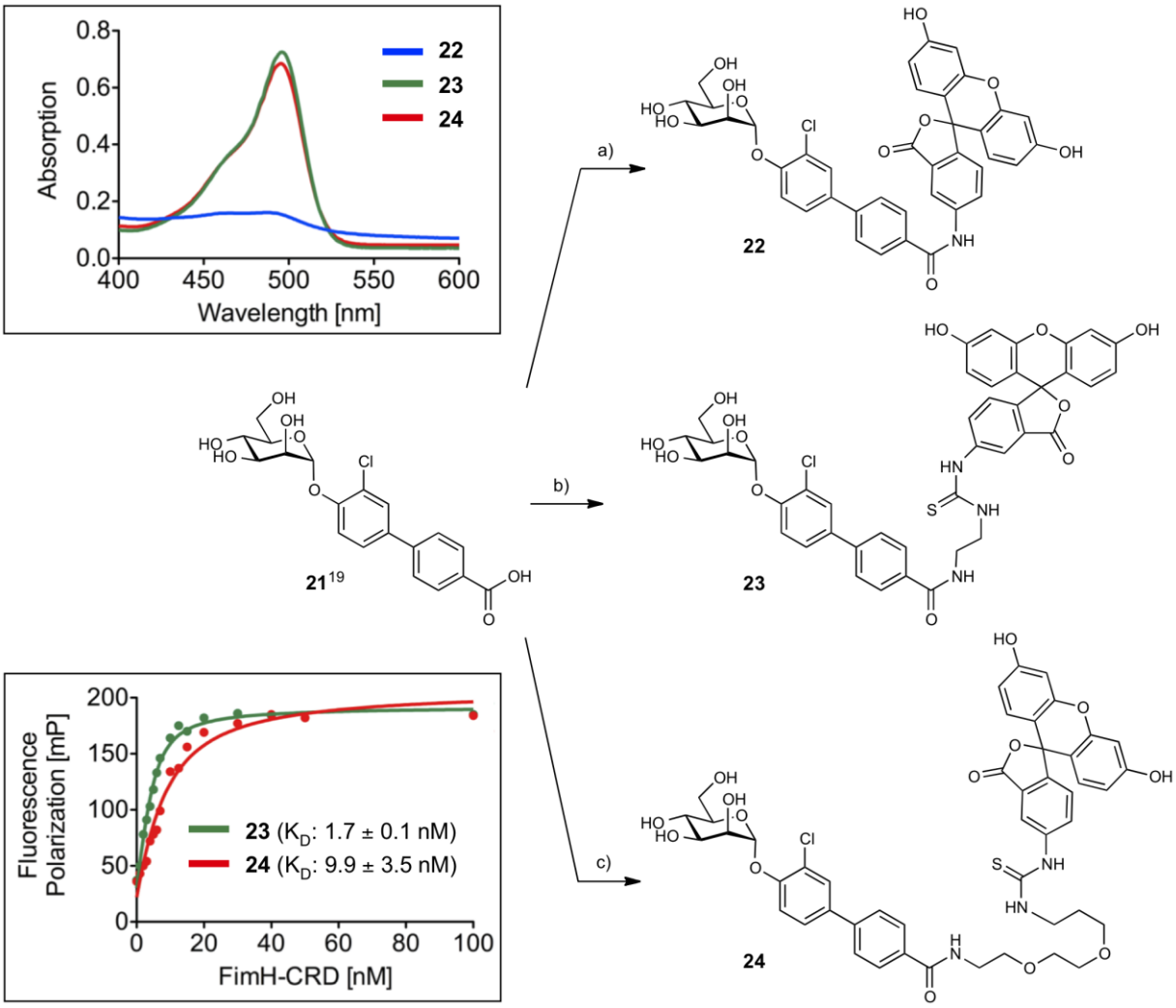

Scheme 4. a) 1-[(1-(Cyano-2-ethoxy-2-oxoethylideneaminooxy)-dimethylamino-morpholinomethylene)] methanaminium hexafluorophosphate (COMU), NEt_3, fluoresceinamine, DMF, rt, 7 h (**22**, 19%); b) i. DIC, NHS, *N*-Boc-ethylenediamine, DMF, rt, 12 h; ii. TFA, DCM, rt, 10 min (68% over two steps), iii. fluorescein isothiocyanate (FITC), NEt_3, DMF, rt, 3 h (**23**, 48%); c) i. DIC, NHS, *N*-Boc-PEG2-NH_2, DMF, rt, 14 h; ii. TFA, DCM, rt, 30 min (62% over two steps); iii. FITC, DMF, rt (**24**, 65%).

For the determination of their binding affinity, fixed concentrations of the reporter ligands **23** and **24** were incubated for 24 h with a linear dilution of the FimH-CRD (0-100 nM). FP was measured using a plate reader, with polarized excitation at 485 nm, and emission at 528 nm measured through appropriately oriented polarizers. Fitting the single-site binding function of Cooper[49] to the observed FP data resulted for compound **23** in a dissociation constant (K_D = 1.7

nM, Figure 3A) similar to that of the unlabeled parent compound **21**,[19] whereas **24** showed a five-fold lower affinity (9.9 nM) (Scheme 4). Therefore, the reporter ligand **23** fulfills all characteristics as an optimal competitor and was used for the FP assay.

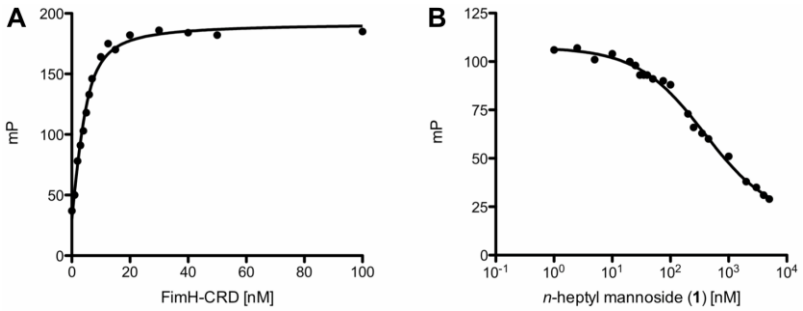

Figure 3. A) Direct binding curve of the labeled competitor **23** obtained by adding a linear dilution of FimH-CRD (0-100 nM) and a constant concentration of competitor **23** (5 nM). The K_D was determined by fitting the experimental data to a single-site binding fit that accounts for ligand depletion. In three FP based direct binding experiments the K_D of competitor **23** was determined to be 1.7 nM. B) Inhibition curve of *n*-heptyl mannoside (**1**) from the competitive FP assay. The IC_{50} value was determined by nonlinear least-squares fitting to a standard 4-parameter equation. A modified Cheng-Prusoff equation[45] was used to calculate the corresponding K_D value (K_D = 28.3 nM).

For the test compounds **1**, **3**, **9**, **20**, and **10a-j**, a 24 h incubation time was applied before FP was measured due to the long residence time of FimH antagonists ($t_{1/2}$ > 3.5 h, Figure 3B[50]). The 24 h incubation period was empirically determined to be necessary to reach equilibrium between reporter ligand and compound of interest. IC_{50} values were obtained by nonlinear least-squares regression (standard four-parameter dose response curve) and converted to K_D values using a modified Cheng-Prusoff equation.[45] This equation accounts for the ligand depletion effect in competitive titrations involving high-affinity interaction partners present in similar concentrations. Under these conditions, the free concentration of an interacting species cannot be assumed to equal the total concentration.

The K_D values determined for the test compounds **1**, **3**, **9**, **20**, and **10a-j** are summarized in Table 1. Against our expectations, the biphenyl mannosides **3** and **9** exhibit similar affinities (Table 1), despite the presence of an electron withdrawing carboxylate substituent in antagonist **9**. According to the crystal structure of FimH co-crystallized with the sulfonamide derivative **10e** (Figure 4A), the outer aromatic ring of the biphenyl aglycone forms π-π interactions with the electron rich Tyr48, which is part of the tyrosine gate of FimH.[15] A reduction of electron density of the aglycone by the electron withdrawing carboxylate was expected to enforce these π-π stacking interactions and lead to improved affinity. However, this beneficial effect might be compensated by an entropic penalty originating from the improved π-π stacking to Tyr48 that might lead to the reduced flexibility of both protein and antagonist. Furthermore, a beneficial enthalpy effect might be partially compensated by an enthalpy penalty originating from the desolvation of the charged carboxylate in **9**[51] (see also experimental part). Although this substituent is solvent exposed, at least a partial desolvation may be necessary upon antagonist binding. To prove this assumption, we replaced the carboxylate by the corresponding methyl ester (→ **20**)[19] in order to reduce the desolvation penalty and, as predicted by the Hammett constant σ_p,[52] to further improve the π-π stacking. Indeed, a six-fold improvement in affinity was achieved. However, since the methyl ester undergoes rapid enzyme-mediated hydrolysis *in vivo*,[19] it will not be available at the place of action in the urinary bladder. The methyl ester was therefore replaced by metabolically stable bioisosteres[39] exhibiting comparable electron withdrawing properties[52] (Table 1, entries 5-13). The most potent derivatives **10d**, **10e** and **10g** showed affinities in the low nanomolar range.

As previously reported,[22] a chloro substituent in the *ortho*-position of the aromatic ring adjacent to the anomeric oxygen is favorable for affinity and improves the physicochemical

properties relevant for oral bioavailability. Indeed, the corresponding antagonist **10j** was the most potent compound tested in this study.

Table 1. Affinities (K_D) of FimH antagonists to FimH-CRD-Th-His$_6$; dissociation constants (K_D) were determined in a competitive fluorescence polarization assay.

Entry	**Compd**	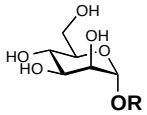	**Affinity** K_D [nM]
1	**1**	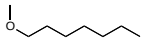	28.3 ± 5.0
2	**3**	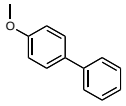	15.1 ± 2.2
3	**9**	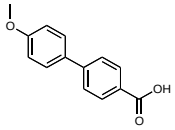	17.9 ± 1.5
4	**20**	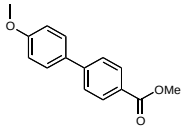	3.6 ± 0.9
5	**10a**	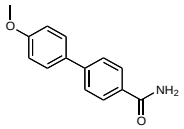	2.8 ± 0.3
6	**10b**	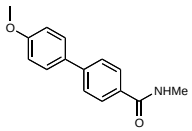	2.9 ± 0.5
7	**10c**	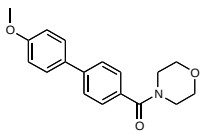	3.0 ± 0.1
8	**10d**	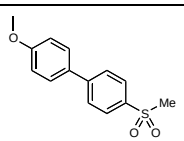	1.7 ± 0.2

9	**10e**	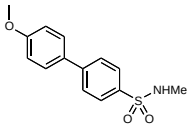	2.7 ± 0.4
10	**10f**	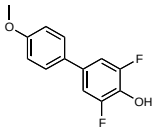	3.7 ± 0.2
11	**10g**	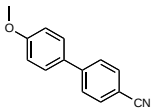	2.0 ± 0.6
12	**10h**	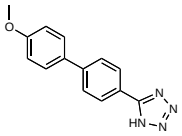	5.7 ± 0.1
13	**10i**	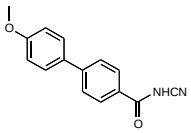	8.4 ± 0.3
14	**10j**	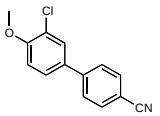	< 1[a)]

[a)] The K_D value of **10j** was approximated to be in the subnanomolar range. The IC_{50} value obtained in the competitive FP assay was equal to the lowest value that can be resolved by the assay, indicating stoichiometric titration of **10j** due to its high affinity. Consequently, its K_D must be below the K_D of competitor **23**.

Isothermal Titration Calorimetry (ITC). To further confirm our hypothesis regarding π-π stacking and desolvation, we performed ITC experiments with the reference compound **1**, the unsubstituted biphenyl mannoside **3**, the carboxylic acid **9**, and the bioisosteres **10b-e, g** and **j** (Table 2). ITC allows the simultaneous determination of the stoichiometry (*N*), the change in enthalpy (ΔH) and the dissociation constant (K_D) for ligand-protein binding.[53,54] The reliable determination of these three parameters requires well-defined sigmoidal titration curves characterized by the dimensionless Wiseman parameter *c* ($c = Mt(0)\ K_D^{-1}$, where $Mt(0)$ is the initial macromolecule concentration).[55] To be sure that data can be fitted with confidence, the

c-value should be between 1 and 1,000 (ideally between 5 and 500),[56] which could be achieved for the antagonists **3** and **9**. For titrations involving low micromolar *Mt*(0) and interactions in the low nanomolar or picomolar range, as suggested for the bioisosteres **10b-j**, *c*-values above 1,000 were expected. Since these conditions lead to steep titration curves that do not allow the determination of the curve slope representing $1/K_D$, we applied an alternative, competitive format referred to as displacement assay.[57,58] First, FimH-CRD-Th-His_6 was pre-incubated with the low affinity antagonist *n*-heptyl 2-deoxy-α-D-mannopyranoside (**25**, for synthesis see supporting information). The high-affinity bioisosteres of interest were titrated into the protein-ligand complex giving well-defined sigmoidal titration curves.

Table 2. Thermodynamic parameters from ITC for selected FimH-antagonists binding to FimH-CRD-Th-His_6; *n*, stoichiometric correction factor; CI, confidence interval from fitting.

Entry	Compd	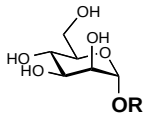	K_D[a] [nM]	Δ*G* [kJ/mol]	Δ*H*[a] [kJ/mol]	-*T*Δ*S* [kJ/mol]	*n*	Type of measurement
1	**1**[b,c]	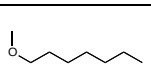	28.9 (25.8 – 32.3)	-43.0	-50.3 (-50.2 – -50.7)	7.3	1.00	direct
2	**3**[b]	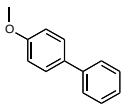	17.7 (14.1 – 22.3)	-44.2	-45.0 (-44.5 – -45.6)	0.8	1.07	direct
3	**9**	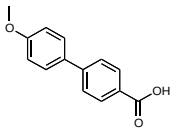	15.0 (13.4 – 16.7)	-44.7	-48.7 (-48.4 – -49.0)	4.0	1.05	direct
4	**10b**	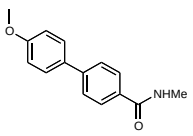	4.3 (3.2 – 5.6)	-47.8	-54.5 (-54.1 – -54.9)	6.7	1.02	competitive vs. **25**
5	**10c**	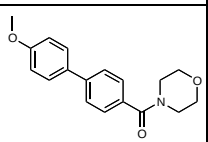	5.0 (3.8 – 6.6)	-47.4	-54.5 (-54.1 – -54.8)	7.1	0.97	competitive vs. **25**

6	**10d**	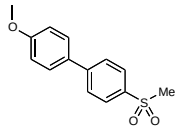	3.0 (2.1 – 4.2)	-48.7	-52.3 (-51.5 – -53.1)	3.6	0.99	competitive vs. **25**
7	**10e**	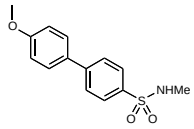	3.5 (2.9 – 4.3)	-48.2	-52.2 (-51.6 – -52.8)	3.9	1.06	competitive vs. **25**
8	**10g**	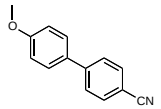	2.8 (2.3 – 3.3)	-48.8	-58.2 (-57.8 – -58.6)	9.4	1.00	competitive vs. **25**
9	**10j**	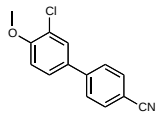	1.3 (1.1 – 1.6)	-50.7	-60.9 (-60.4 – -61.4)	10.1	1.01	competitive vs. **25**
10	**25**	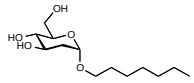	9’386 (8’555 – 10’287)	-28.7	-19.5 (-19.1 – -20.0)	-9.1	1.00	direct

[a] 95% confidence interval from fitting in parentheses; [b] Global fit including two direct titration measurements; [c] ITC data were previously published with an *n*-value of 0.82.[37]

The resulting K_D values (Table 2) correspond well with the data obtained from the FP assay (Table 1). A comparison of the thermodynamic fingerprints of antagonists **3** and **9** reveals that the more favorable enthalpic contribution resulting from facilitated π-π stacking leads to a net enthalpy gain ($\Delta\Delta H$: -3.7 kJ/mol). However, an even greater increase in enthalpy is likely countered by the enthalpy costs for desolvation of the electron withdrawing carboxylate.

The gain in enthalpy is in turn compensated by an unfavorable entropy ($-T\Delta\Delta S$: 3.2 kJ/mol) as a result of the reduced flexibility of both the antagonist and the Tyr48 side-chain caused by the improved interaction. This is not entirely outweighed by the beneficial entropy contribution related to the partial desolvation of the carboxylate and the related release of water into the bulk. Added together, the enthalpy and entropy contributions of antagonists **3** and **9** result in

similar affinities (K_D: 17.7 and 15.0 nM, respectively).

In contrast, the replacement of the carboxylate group by various neutral bioisosteres (entries 4-7) reduces the enthalpy costs for desolvation (see calculated free energies of desolvation, experimental part) and therefore leads to a markedly improved enthalpy ($\Delta\Delta H$: -3.5 to -5.8 kJ/mol). As a result, an up to fivefold improvement of the K_D values was achieved. Finally, with a cyano substituent (entries 8 & 9), the enthalpy term was further improved ($\Delta\Delta H$: -3.7 kJ/mol) due to a reduced desolvation penalty and improved π-π stacking interactions. However, this beneficial component is again partially compensated by a decrease in entropy. This can be attributed, first, to the loss of flexibility of the tightly bound ligand (Figure 4B) and, second, to the smaller surface area of the cyano substituent compared to amide, sulfonamide and sulfone, which results in a smaller number of water molecules being released to bulk upon binding.

X-ray Crystallography. To determine the binding poses of the bioisosters, we co-crystallized the compounds **10e** and **10j** with the FimH-CRD (Figure 4). Atomic resolution crystal structures were obtained at 1.07 Å (**10e**) and 1.10 Å (**10j**). As observed in previous mannoside co-crystal structures,[15,18,36] the mannose moiety forms an extensive hydrogen bond network to the well-defined binding site with all of its hydroxyl groups. The biphenyl aglycone is located between the tyrosine gate residues (Tyr48/Tyr137). The π-π stacking of the second aromatic ring of the aglycone to the side chain of Tyr48 contributes most to the interaction energy of the aglycone moiety. Interactions to the Tyr137 side-chain on the other hand are only limited. Whereas a previously published crystal structure of a biphenyl mannoside in complex with FimH-CRD suffers from crystal contacts of binding site residues (Tyr48 side-chain to backbone oxygen of Val27) possibly causing the distortion of the binding site,[18] the binding site of our structures are mostly solvent exposed. This revealed the flexibility of the aglycone

in the FimH-CRD/**10e** structure, since the electron density towards the solvent-exposed sulfonamide indicates that there is not one single orientation. Therefore, the aglycone was modeled in two distinct poses. In contrast, in the FimH-CRD/**10j** structure the amino acid side chain of Y48 can be modeled in two distinct rotamers, suggesting flexibility also of the receptor.

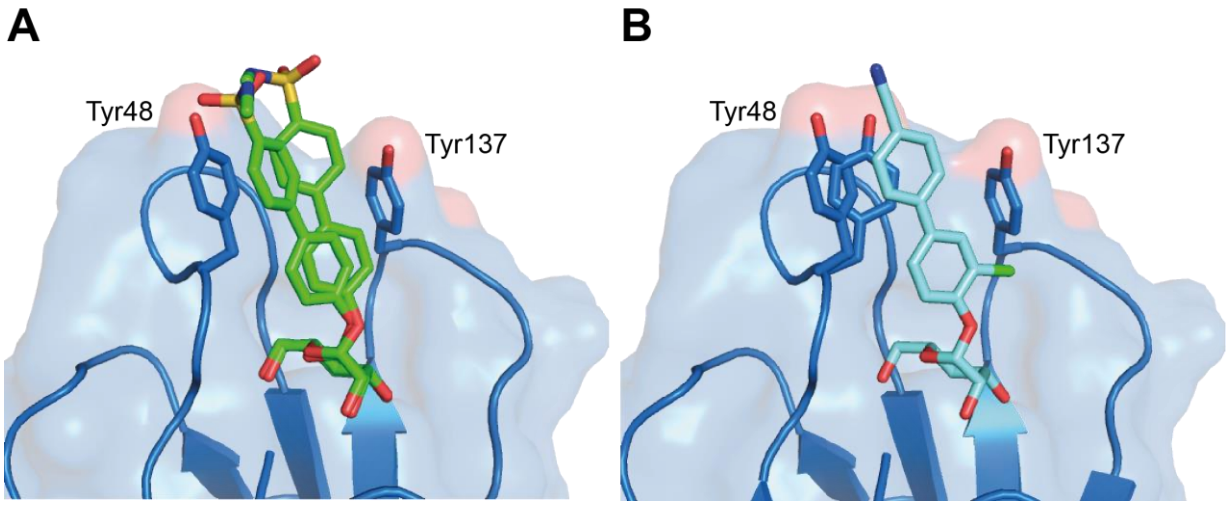

Figure 4. Ligand binding poses determined by X-ray co-crystallization with compounds **10e** resolved to 1.07 Å (**A**) and **10j** resolved to 1.10 Å (**B**). The electron density surrounding the aglycone of **10e** indicates flexibility of the aglycone and was modeled in two poses. Both compounds bind in a similar pose with a well-defined hydrogen network surrounding the mannose moiety and π-π stacking interactions between the second aromatic ring and Tyr48 side-chain (**A**). In contrast, in the FimH-CRD/**10j** structure the amino acid side chain of Y48 can be modeled in two distinct rotamers, suggesting flexibility also of the receptor (**B**).

Physicochemical Properties and *In Vitro* Pharmacokinetics. Intestinal absorption and renal excretion are prerequisites for a successful oral treatment of UTI with FimH antagonists. Furthermore, reabsorption of antagonist from the renal ultrafiltrate is desirable for maintaining the minimal anti-adhesive concentration in the target organ, namely the bladder, over an extended period of time. To estimate the influence of the bioisostere approach on oral bioavailability and the rate of renal excretion, we determined lipophilicity by means of the

octanol-water distribution coefficient (log $D_{7.4}$),[59] aqueous solubility, and membrane permeability in the artificial membrane permeability assay (PAMPA)[60] and the colorectal adenocarcinoma (Caco-2) cell monolayer model.[61]

Table 3. Physicochemical and *in vitro* pharmacokinetic parameters.

Compd	pK_a [a]	log $D_{7.4}$ [b]	Solubility [µg/mL] / pH [c]	PAMPA log P_e [cm/s] / pH [d]	Caco-2 P_{app}, [10^{-6} cm/s] [e]		PPB f_b [%] [f]	Metabolic stability $t_{1/2}$ [min] [g]
					a→b	b→a		
1	---	1.65	> 3000	-4.89	7.0 ± 0.6	9.4 ± 0.2	81	13
3	---	2.1 ± 0.1	21 ± 1 / 7.4	-4.7 ± 0.1 / 7.4	10.0 ± 0.9	19.0 ± 1.2	93 ± 1	n.d.
20	---	2.14	33.8 / 6.51	-4.7	4.23	n.d.	93	1.0
9	3.88	< -1.5	> 3000 / 6.61	no permeation	n.d.	n.d.	73	> 60
10a	---	0.5 ± 0.1	12 ± 1 / 7.4	-6.8 ± 0.3 / 7.4	0.12 ± 0.01	0.61 ± 0.03	n.d.	n.d.
10b	---	0.8 ± 0.0	122 ± 13 / 7.4	-9.2 ± 1.4 / 7.4	1.10 ± 0.82	0.87 ± 0.15	n.d.	n.d.
10c	---	0.2 ± 0.1	> 250 / 7.4	-7.8 ± 0.3 / 7.4	0.18 ± 0.07	1.30 ± 0.03	48 ± 2	> 60
10d	---	0.4 ± 0.0	246 ± 17 / 7.4	-7.2 ± 0.0 / 7.4	0.36 ± 0.01	1.76 ± 0.12	99 ± 1	> 60
10e	---	0.7 ± 0.1	> 250 / 7.4	-8.6 ± 0.2 / 7.4	0.28 ± 0.23	1.82 ± 0.14	> 99	> 60
10f	6.5	1.1 ± 0.0	> 150 / 3.0 > 150 / 7.4	-7.7 ± 0.8 / 5.0 -8.8 ± 0.1 / 7.4	0.40 ± 0.02	1.90 ± 0.17	n.d.	n.d.
10g	---	1.4 ± 0.0	186 ± 4 / 7.6	-5.7 ± 0.0 / 7.4	2.0 ± 0.1	13.2 ± 2.1	99 ± 0	> 60
10h	3.7	-1.4 ± 0.1	11 ± 0 / 3.0 273 ± 2 / 7.4	-9.3 ± 1.4 / 5.0 -8.8 ± 1.4 / 7.4	0.17 ± 0.00	0.22 ± 0.01	n.d.	n.d.
10i	2.5	-1.1 ± 0.1	> 150 / 3.0 > 150 / 7.4	-6.8 ± 0.2 / 5.0 -7.0 ± 0.1 / 7.4	0.22 ± 0.14	0.29 ± 0.03	n.d.	n.d.
10j	---	2.1 ± 0.0	192 ± 5 / 7.4	-5.2 ± 0.0 / 7.4	2.2 ± 0.4	22.1 ± 1.5	89 ± 1	> 60

a) pK_a values were determined by NMR spectroscopy; b) Octanol-water distribution coefficients (log $D_{7.4}$) were determined by a miniaturized shake-flask procedure at pH 7.4, values represent the mean ± SD of sextuplicate measurements;[59] c) Kinetic solubility was measured in a 96-well format using the µSOL Explorer solubility analyzer at the indicated pH in triplicate; d) P_e = effective permeability: passive permeation through an artificial membrane was determined by the parallel artificial membrane permeation assay (PAMPA), values represent the mean ± SD of quadruplicate measurements performed at the indicated pH;[60] e) P_{app} = apparent permeability: permeation through a Caco-2 cell monolayer was assessed in the absorptive (a→b) and secretory (b→a) directions

in triplicate;[61] f) Plasma protein binding (PPB) was determined by equilibrium dialysis in triplicate;[62] g) Metabolic stability was determined by incubating the compounds (2 µM) with pooled rat liver microsomes (RLM, 0.5 mg/mL) in presence of NADPH (1 mM, compounds **1**, **9, 10c-e**, **g**, **j**) or without NADPH (compound **20**);[63] n.d. = not determined.

Oral Bioavailability. Oral bioavailability of a compound relies on solubility, permeation through the membranes lining the intestine, and stability against first pass metabolism.[64,65] As discussed by Lipinski[66] and Curatolo,[67] dose and permeability define the minimum aqueous solubility required for oral administration. Thus, a dose of 1 mg/kg of a moderately permeable compound requires a solubility of at least 52 µg/mL. Whereas sufficient aqueous solubility (> 3000 µg/mL) was reported for *n*-heptyl α-mannopyranoside (**1**),[19] the unsubstituted biphenyl α-D-mannopyranoside **3** as well as the antagonists bearing a methylcarboxylate, carboxamide, or tetrazole substituent (compounds **20**, **10a** and **10h**) were found to be scarcely soluble.[22] As proposed by Ishikawa,[68] a possible reason is the apolar and planar aglycone. By contrast, the polar carboxylic acid moiety present in antagonist **9** or the substituents in the bioisosteres **10b-j** enhance solubility to 122-273 µg/mL, a level sufficient for *in vivo* PK studies. For *in vivo* disease studies, however, dosages of up to 10 mg/kg were foreseen (see below), requiring a solubility of 520 µg/mL.[66,67] For this reason, surfactant Tween 80 (1%) had to be added.

Furthermore, permeability data derived from PAMPA[69] and the Caco-2 model[70] suggest moderate to high permeation of the moderately lipophilic antagonists **1**, **3** and **20** (log $D_{7.4}$ > 1.6) through the intestinal membranes. The bioisosteres **10a-f**, **h**, **i**, although slightly more permeable than the strongly hydrophilic carboxylic acid derivative **9**, show only low values of permeability compared to *n*-heptyl α-D-mannopyranoside (**1**) or the unsubstituted biphenyl mannoside **3**. However, the *para*-cyanobiphenyl derivatives **10g** and **10j** display elevated log $D_{7.4}$ and effective permeability (log P_e) in the range for successful intestinal absorption.

Regarding both, sufficient aqueous solubility and elevated membrane permeability, the *para*-cyano substituted bioisosteres **10g** and **10j** are thus the most promising candidates for oral absorption. Moreover, combining the bioisosteric replacement with the addition of a chloro substituent in the *ortho*-position of the aromatic ring adjacent to the anomeric oxygen (→ **10j**)[22] resulted in the most advantageous physicochemical profile for oral bioavailability.

Renal Excretion. The rate of renal excretion depends on the rate of glomerular filtration and the propensity to tubular secretion and reabsorption of an antagonist.[71] Only the fraction that is not bound to plasma proteins is expected to enter the glomerular filtrate.[72] Plasma protein binding (PPB) data indicating the fraction bound (f_b) are listed in Table 2.[62] The biphenyls **9** and **10c** were identified as moderate binders to plasma proteins ($f_b \leq 65\%$), which suggests a low impact of PPB on antagonist filtration. The f_b values of the antagonists **1**, **3**, **20** and **10j** were between 80 and 93%, whereas the bioisosteres **10d**, **e** and **g** showed particularly high protein binding ($f_b \geq 99\%$) implying slow compound entry into the primary urine. However, the kinetic aspects of PPB, that is, association and dissociation rate constants, remain to be determined to quantify precisely the influence of PPB on filtration.[73]

Furthermore, log $D_{7.4}$ was identified as key determinant of tubular reabsorption.[74-76] Accordingly, lipophilic compounds are predominantly reabsorbed from the renal filtrate. Given that renal clearance is the major route of elimination, this will result in a slow but steady excretion into the bladder. In contrast, hydrophilic compounds are poorly reabsorbed and thus quickly renally eliminated, which leads to high initial compound levels in the urine but narrows the time range where the minimal anti-adhesive concentration is maintained. Consequently, low log $D_{7.4}$ as shown for the antagonists **9**, **10h** and **10i** implies low tubular reabsorption and rapid elimination of the filtered molecules by the urine. Otherwise, log $D_{7.4}$

between 0.2 and 0.7, such as determined for the bioisosteres **10a-e,** suggests increasing propensity to tubular reuptake, whereas log $D_{7.4}$ > 1 as shown for heptyl mannoside **1** and the biphenyl mannosides **3**, **20**, **10g**, **10f** and **10j** is optimal for tubular reabsorption from the glomerular filtrate and thus for slow renal clearance.

Metabolic Stability. Increasing lipophilicity is usually paralleled by increasing susceptibility to metabolism.[77] Liabilities towards metabolic clearance pathways which prevent the intact antagonist from reaching the target in the bladder were therefore of interest. To assess their propensity to cytochrome P450 (CYP450)-mediated metabolism, heptyl mannoside **1**, the carboxylic acid derivative **9**, and the bioiosteres **10c-e**, **g**, **j** were incubated with rat liver microsomes (RLM, 0.5 mg/mL) in presence of the cofactor β-nicotinamide adenine dinucleotide phosphate (NADPH).[63] To confirm the high propensity of the methyl ester present in antagonist **20** to carboxylesterase (CES)-mediated hydrolysis, this antagonist was incubated with RLM only. The profiles of unchanged compound versus time revealed high susceptibility of heptyl mannoside **1** to CYP450-mediated metabolism ($t_{1/2}$ = 13 min) and rapid hydrolysis of the ester **20** by the hepatic CES ($t_{1/2}$ = 1.0 min). Otherwise, the bioisosteres **10c**-**e**, **g** & **j** were stable against enzyme-mediated bioconversion ($t_{1/2}$ > 60 min) suggesting lower propensity to metabolic, non-renal elimination pathways.

Considering PPB, lipophilicity, and metabolic stability data, we therefore expected (i) a steady release of compounds **10d**, **e**, **g**, **j** into the bladder because of high PPB decelerating glomerular filtration (**10d**, **e**, **g**) and/or high log $D_{7.4}$ supporting tubular reabsorption (**10g**, **j**), (ii) a fast excretion of antagonists **9** and **10c** via the urine due to low PPB and low log $D_{7.4}$, and (iii) a rapid clearance of heptyl mannoside **1** from the body by renal and metabolic pathways.

Compounds featuring high propensity to renal excretion as major route of elimination (**10c**, **10e** and **10j**) were selected for *in vivo* PK studies in a mouse model.

Pharmacokinetic Studies in C3H/HeN Mice. This first part of our study explored the predicted effects of lipophilicity, PPB, and metabolic stability on antagonist disposition and elimination upon a single dose i.v. application (50 mg/kg) of compounds **10c** and **10e**. The PK parameters of these applications and those of the previously published carboxylate **9** are summarized in Table 4. The Table also contains the results of the i.v. administration of compound **10j** (0.625 mg/kg).

Table 4. Pharmacokinetic parameters determined after a single iv application of compounds **9**, **10c**, **10e** and **10j** in female C3H/HeN mice. Values were calculated using PKSolver.[78] C_0, initial concentration; V_z, volume of distribution in terminal phase; AUC, Area under the curve; CL_{tot}, total clearance; C_{max}, maximal concentration.

Compd	**Plasma**						**Urine**
	C_0 (µg/mL)	Dose (mg/kg)	V_z (mL)	$t_{1/2}$ (h)	$AUC_{0\text{-}inf}$ (µg x h/mL)	CL_{tot} (mL/h)	C_{max} (µg/mL)
9	40	50	25.2	0.33	23.5	53.1	300
10c	109.7	50	28.3	0.4	25.3	49.4	4611
10e	151.6	50	19.5	1.9	175.1	7.1	387
10j	0.36	0.625	52.8	0.17	0.07	218	10

In contrast to the fast plasma clearance of antagonists **9** and **10c** (Figure 5A), the methyl sulfonamide bioisostere **10e** attained higher initial concentration in plasma (C_0) and lower total clearance (CL_{tot}). Therefore, it could be detected until 6 h post application, resulting in markedly higher plasma AUC. The observed high C_0 of compound **10e** may be attributed to a small volume of distribution (V_z) resulting from the high PPB ($f_b \geq 99\%$).[72] In urine (Figure 5B), the carboxylic acid **9** and the morpholinomethanone **10c** displayed high levels immediately following administration and a rapid concentration decrease within the first two

hours, reflecting the rapid elimination from plasma. Fast renal excretion as major route of elimination can be rationalized by the physicochemical properties of the antagonists **9** and **10c**, that is, moderate PPB and log $D_{7.4}$, as well as high metabolic stability. Otherwise, the methyl sulfonamide bioisostere **10e** showed sustained compound levels in urine over a period of 2 h and subsequent slow decrease until 6 h post administration. This sustained renal excretion is a result of the interplay of the antagonist's elevated PPB and log $D_{7.4}$.

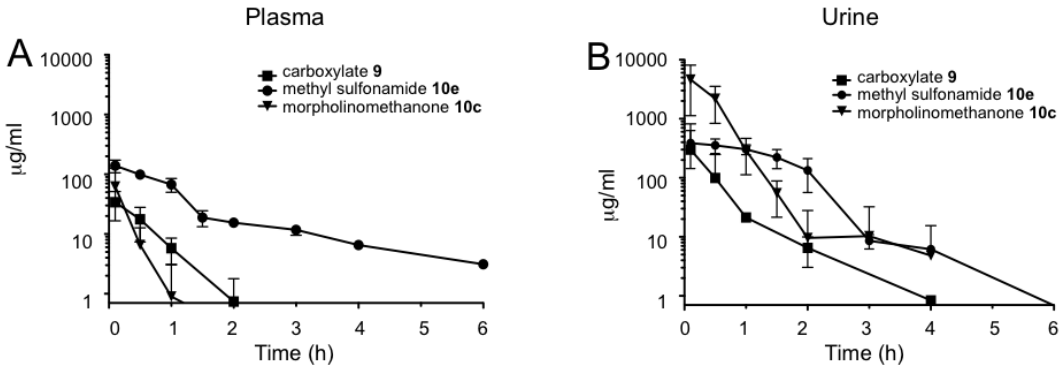

Figure 5. Antagonist concentrations in (A) plasma and (B) urine after a single i.v. application of **9**, **10c**, and **10e** (50 mg/kg).

In a second study, the *para*-cyano bioisostere **10j**, characterized by a high oral absorption potential, was administered as a single dose i.v. (0.625 mg/kg) and p.o. (1.25 mg/kg). The plasma concentration curve upon i.v. dosing displays a steep decline within the first hour post application, while the p.o. curve shows a prolonged period where absorption and elimination are in equilibrium (Figure 6A). The urine concentration profiles (Figure 6B) parallel the plasma curves obtained by the two modes of application, i.e. high plasma clearance upon i.v. bolus injection led to high initial antagonist levels in urine and a rapid concentration decline. By contrast, sustained plasma concentrations upon p.o. administration resulted in prolonged urine levels.

As a result, urine concentrations exceed the minimum level required for the anti-adhesive effect as estimated from the *in vitro* cell infection model[79] (minimal anti-adhesion concentration[23], $MAC_{90,}$ 0.094 µg/mL) for more than eight hours upon oral single-dose administration (Figure 6B).

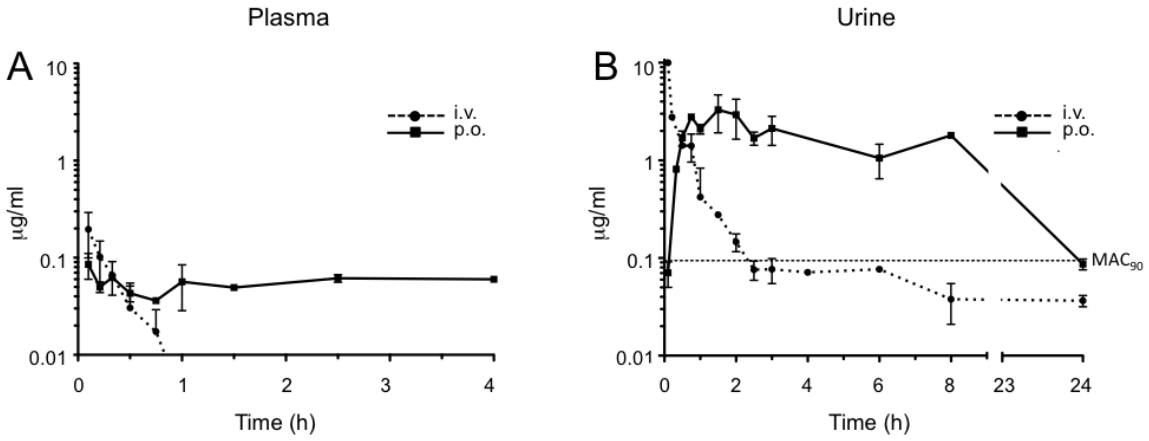

Figure 6. Antagonist concentrations in (A) plasma and (B) urine after a single i.v. and p.o. application of compound **10j** (i.v.: 0.625 mg/kg; p.o.: 1.25 mg/kg). MAC_{90}, minimal anti-adhesive concentration to inhibit 90% adhesion (0.094 µg/mL).

Infection study in C3H/HeN Mice. In a preventive study, six mice were inoculated with UTI89 following an oral application of **10j** (1.25 mg/kg) 40 min prior to infection. Three hours after inoculation, the animals were sacrificed and bladder and kidneys were removed. Organs were homogenized and analyzed for bacterial counts. The effect of the FimH antagonist was compared to a 8 mg/kg dose of ciprofloxacin (CIP), applied subcutaneously (s.c.) ten minutes before infection. CIP is used as standard antibiotic therapy in humans for the treatment of UTI.[80] In mice, the dose of 8 mg/kg s.c. was shown to mimic the standard human dose regarding peak levels and the AUC_{24} in serum.[81] The median reductions in bacterial counts in mice treated with **10j** and CIP compared to the control group three hours after infection are displayed in Figure 7.

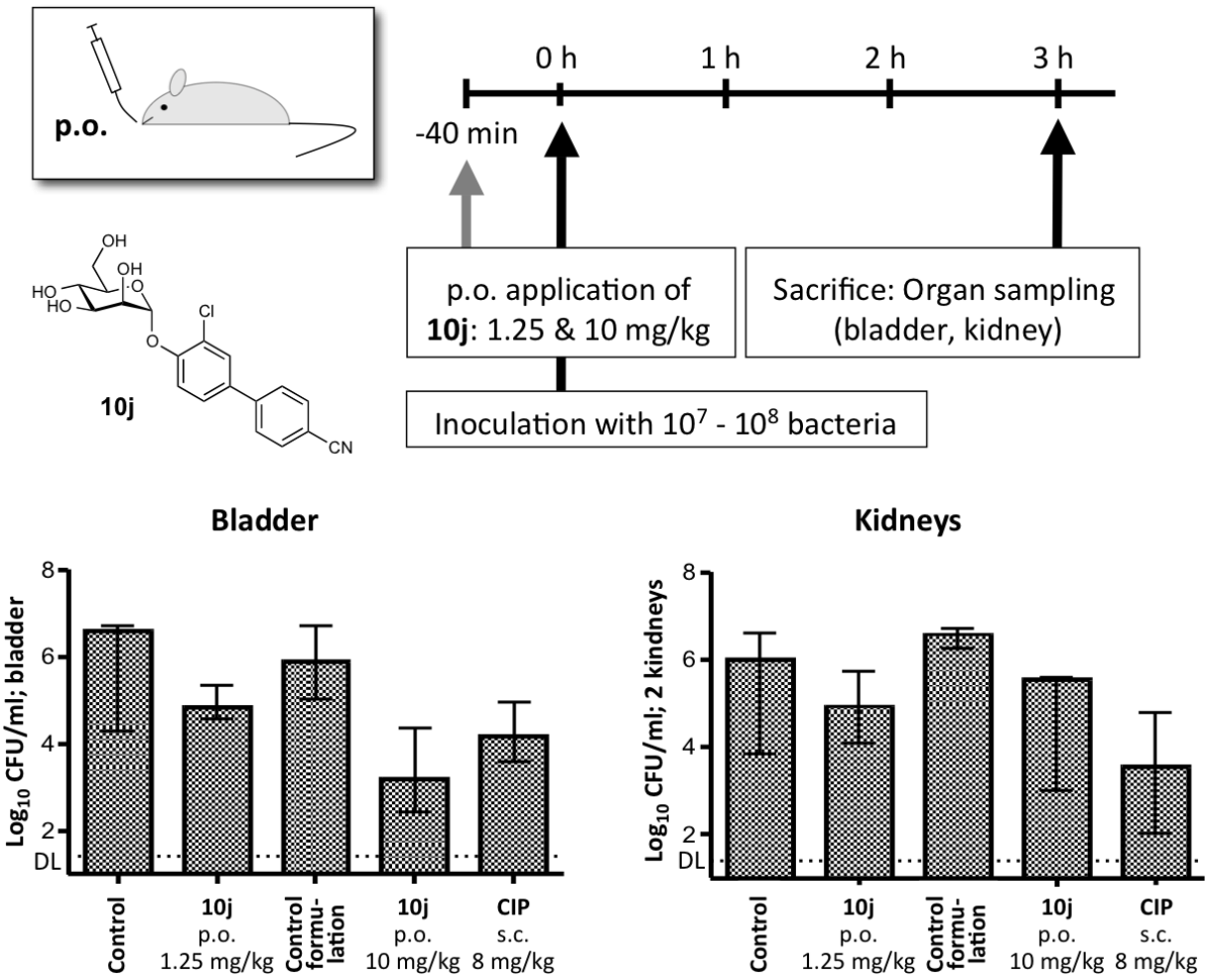

Figure 7. Preventive efficacy of **10j** in the UTI mouse model 3 h after infection. The bars depict the median bacterial load with the interquartile range in the different study groups. Shown are the results of the control group (PBS), control group formulation (5% DMSO in PBS containing 1% Tween 80), and the intervention groups with the preventive applications of either, 1.25 mg/kg or 10 mg/kg **10j** p.o. or 8 mg/kg CIP s.c. (representing the murine dose equivalent to a human standard dose).[81] DL, detection limit; CFU, colony forming units.

The median value in the untreated control group showed bacterial counts of 6.6 $\log_{10}$ colony forming units (CFU) in the bladder and 6 $\log_{10}$ CFU in the kidneys. After oral application of 1.25 mg/kg of **10j**, bacterial loads in the bladder decreased by 1.78 $\log_{10}$ CFU and 1.07 $\log_{10}$ CFU in the kidneys. The lower reduction in the kidneys is most likely due to the differing adhesion mechanisms between bladder and kidneys (type 1 pili vs P-pili), which is not targeted by **10j**.[82] With CIP (8 mg/kg s.c.) a substantial reduction in both, bladder and kidneys (median

reductions of 2.44 $\log_{10}$ and 2.47 $\log_{10}$, respectively) was observed. Despite the low oral dose of **10j** (1.25 mg/kg), the approximately 100-fold reduction of CFU in the bladder promised an even higher effect upon dose increase to 10 mg/kg. Since the solubility of **10j** for this increased dose is too low (192 µg/mL), we used 5% DMSO and surfactant Tween 80 (1%) as solubilizer. To effectively compare the effect of a higher dose of **10j**, a control group receiving the formulation only (5% DMSO in PBS containing 1% Tween 80, termed control group formulation) was tested in parallel. When 10 mg/kg of **10j** were applied, bacterial loads in the bladder decreased by 2.68 $\log_{10}$ CFU/mL compared to the control group formulation, clearly exceeding the effect of CIP with a reduction of 2.44 $\log_{10}$ CFU/mL. However, only a moderate reduction of 1.04 $\log_{10}$ CFU was achieved in the kidneys.

SUMMARY AND CONCLUSION

Recently, numerous monovalent alkyl and aryl α-D-mannopyranosides have been described as potent FimH antagonists. However, most of them suffer from insufficient pharmacokinetic properties, i.e. modest bioavailability and short duration of the therapeutic effect in the bladder, their site of action. As a consequence, high doses at short intervals are required to achieve anti-adhesive effects over an extended period of time. Therefore, the goal of the present study was an appropriate optimization of the pharmacokinetic profile of biphenyl α-D-mannopyranosides while keeping their high affinity to the CRD of FimH. The starting point was the biphenyl-carboxylate **9** where the critical carboxylate was replaced by bioisosteres.[39,83] With a series of bioisosteres, a three- to fivefold improvement of affinity was achieved compared to **9**. Although binding necessitates only partial desolvation of the carboxylate and its bioisosteric replacements, a reduction of the enthalpy penalty for desolvation[51] was identified as the source of the improved affinity exhibited by the bioisosteres. Thermodynamic

evaluation of antagonists **10b-e** revealed almost identical enthalpy contribution to binding. However, for antagonists with the *para*-cyano substituent (**10g** & **10j**) an enhancement of up to -8.7 kJ/mol was observed, indicating a reduced desolvation penalty and an improved stacking as derived from the crystal structure of **10j** co-crystallized with the CRD of FimH (Figure 4B). On the other hand, higher affinity originating from a reduction of conformational flexibility of ligand and protein resulted in a concomitant entropy penalty of up to 6.5 kJ/mol.

In addition to the improved pharmacodynamics, the relevant pharmacokinetic parameters (solubility, permeability, renal excretion) were substantially improved. With 3'-chloro-4'-(α-D-mannopyranosyloxy)-biphenyl-4-carbonitrile (**10j**), a FimH antagonist with an optimal *in vitro* PK/PD profile was identified. The *para*-cyano substituent conferred lipophilicity and high binding to plasma proteins, which slowed down the rate of renal excretion. Despite higher lipophilicity, antagonist **10j** was insusceptible to CYP450-mediated metabolism, and therefore predominantly eliminated via the renal pathway. *In vivo* experiments confirmed the excellent PK-profile of **10j** with steady renal excretion for more than 8 h after oral application (1.25 mg/kg), suggesting a long-lasting anti-adhesive effect. Finally, the preventive oral application of **10j** (10 mg/kg) reduced the bacterial load in the bladder by almost 1000-fold three hours after infection. Although the first three hours of the infection do not represent the complete infection cycle, they represent the time span of bacteria adhering and invading urothelial cells.[84,85] Nevertheless, the effect of FimH antagonist **10j** within a longer infection time and at higher dosing will be the subject of future investigations.

EXPERIMENTAL SECTION

Synthesis

The synthesis of compounds **10a-d**, **10f**, **10g**, **10i**, **13a-d**, **13f**, **13g**, **15**, **18** and **25**, including compound characterization data, can be found in the Supporting Information.

General methods. NMR spectra were recorded on a Bruker Avance DMX-500 (500.1 MHz) spectrometer. Assignment of ^{1}H and ^{13}C NMR spectra was achieved using 2D methods (COSY, HSQC, HMBC). Chemical shifts are expressed in ppm using residual $CHCl_3$, CHD_2OD or HDO as references. Optical rotations were measured using Perkin-Elmer Polarimeter 341. Electron spray ionization mass spectra (ESI-MS) were obtained on a Waters micromass ZQ. The LC/HRMS analysis were carried out using a Agilent 1100 LC equipped with a photodiode array detector and a Micromass QTOF I equipped with a 4 GHz digital-time converter. Microwave-assisted reactions were carried out with a CEM Discover and Explorer. Reactions were monitored by TLC using glass plates coated with silica gel 60 F_{254} (Merck) and visualized by using UV light and/or by charring with a molybdate solution (a 0.02 M solution of ammonium cerium sulfate dihydrate and ammonium molybdate tetrahydrate in aqueous 10% H_2SO_4). MPLC separations were carried out on a CombiFlash Companion or Rf (Teledyne Isco) equipped with RediSep normal-phase or RP-18 reversed-phase flash columns. LC-MS separations were done on a Waters system equipped with sample manager 2767, pump 2525, PDA 2525 and micromass ZQ. All compounds used for biological assays are at least of 95% purity based on HPLC analytical results. Commercially available reagents were purchased from Fluka, Aldrich, Alfa Aesar or abcr GmbH & Co. KG (Germany). Solvents were purchased from Sigma-Aldrich or Acros and were dried prior to use where indicated. Methanol (MeOH) was dried by refluxing with sodium methoxide and distilled immediately

before use. Dimethoxyethane (DME) was dried by filtration over Al_2O_3 (Fluka, type 5016 A basic).

4'-(2,3,4,6-Tetra-*O*-acetyl-α-D-mannopyranosyloxy)-*N*-methyl-biphenyl-4-sulfonamide (13e). A Schlenk tube was charged with aryl iodide **11**[22] (116 mg, 0.21 mmol), 4-(*N*-methylsulfamoyl)-phenylboronic acid (**12e**, 50 mg, 0.23 mmol), Pd(dppf)Cl_2·CH_2Cl_2 (5 mg, 0.006 mmol), K_3PO_4 (67 mg, 0.32 mmol) and a stirring bar. The tube was closed with a rubber septum and was evacuated and flushed with argon. This procedure was repeated once, and then anhydrous DMF (1 mL) was added under a stream of argon. The mixture was degassed in an ultrasonic bath and flushed with argon for 5 min, and then stirred at 80 °C overnight. The reaction mixture was cooled to rt, diluted with EtOAc (50 mL), and washed with water (50 mL) and brine (50 mL). The organic layer was dried over Na_2SO_4 and concentrated *in vacuo*. The residue was purified by MPLC on silica gel (petroleum ether/EtOAc) to afford **13e** (105 mg, 84%) as a white solid. $[\alpha]_D^{20}$ +56.4 (*c* 0.50, MeOH); ^{1}H NMR (500 MHz, $CDCl_3$): δ = 7.92-7.90 (m, 2H, Ar-H), 7.70-7.68 (m, 2H, Ar-H), 7.57-7.55 (m, 2H, Ar-H), 7.21-7.19 (m, 2H, Ar-H), 5.60-5.57 (m, 2H, H-1, H-3), 5.48 (dd, *J* = 1.8, 3.4 Hz, 1H, H-2), 5.40 (t, *J* =10.0 Hz, 1H, H-4), 4.38 (dd, *J* = 5.4, 10.8 Hz, 1H, NH), 4.30 (dd, *J* = 4.9, 12.3 Hz, 1H, H-6a), 4.13-4.08 (m, 2H, H-5, H-6b), 2.72 (d, *J* = 5.4 Hz, 3H, NCH_3), 2.22, 2.07, 2.05, 2.04 (4 s, 12H, 4 $COCH_3$); ^{13}C NMR (126 MHz, $CDCl_3$): δ = 170.55, 170.06, 170.03, 169.75 (4 CO), 155.97, 144.81, 137.16, 134.09, 128.62, 127.85, 127.39, 117.01 (Ar-C), 95.78 (C-1), 69.34 (C-5), 69.31 (C-2), 68.81 (C-3), 65.86 (C-4), 62.07 (C-6), 29.44 (NH*C*H_3), 20.92, 20.74, 20.72 (4C, 4 CO*C*H_3); ESI-MS: *m/z*: Calcd for $C_{27}H_{31}NNaO_{12}S$ $[M+Na]^+$: 616.1, found: 616.1.

4'-(α-D-Mannopyranosyloxy)-*N*-methyl-biphenyl-4-sulfonamide (10e). To a solution of **13e** (40 mg, 0.07 mmol) in dry MeOH (5 mL) was added freshly prepared 1 M NaOMe/MeOH

(0.1 eq) under argon. The mixture was stirred at rt until the reaction was complete (monitored by TLC), then neutralized with Amberlyst-15 (H^+) ion-exchange resin, filtered and concentrated *in vacuo*. The residue was purified by MPLC on silica gel (DCM/MeOH, 10:1-7:1) to afford **10e** (22 mg, 76%) as white solid. $[\alpha]_D^{20}$ +105.7 (*c* 0.30, MeOH); ^{1}H NMR (500 MHz, CD_3OD): δ = 7.90-7.88 (m, 2H, Ar-H), 7.80-7.79 (m, 2H, Ar-H), 7.66-7.64 (m, 2H, Ar-H), 7.26-7.25 (m, 2H, Ar-H), 5.58 (d, *J* = 1.7 Hz, 1H, H-1), 4.06 (dd, *J* = 1.8, 3.3 Hz, 1H, H-2), 3.96 (dd, *J* = 3.4, 9.5 Hz, 1H, H-3), 3.79-3.74 (m, 3H, H-4, H-6a, H-6b), 3.63 (ddd, *J* = 2.5, 5.2, 9.7 Hz, 1H, H-5), 2.57 (s, 3H, NHC*H*$_3$); ^{13}C-NMR (126 MHz, CD_3OD): δ = 158.34, 146.13, 138.67, 134.55, 129.53, 128.82, 128.21, 118.29 (Ar-C), 100.09 (C-1), 75.53 (C-5), 72.42 (C-3), 71.96 (C-2), 68.32 (C-4), 62.68 (C-6), 29.31 ($NHCH_3$); HRMS: *m/z*: Calcd for $C_{19}H_{23}NNaO_8S$ $[M+Na]^+$: 448.1037, found: 448.1038.

5-(4'-(2,3,4,6-Tetra-*O*-acetyl-α-D-mannopyranosyloxy)-biphenyl-4-yl)-1*H*-tetrazole (14). A Schlenk tube was charged with **13g** (30 mg, 0.06 mmol), trimethylsilyl azide (16 μL, 0.12 mmol), dibutyltin oxide (2 mg, 0.006 mmol), DME (1 mL) and a stirring bar. The mixture was heated to 150 °C for 10 min by microwave irradiation. The reaction mixture was cooled to rt, and then concentrated *in vacuo*. The residue was purified by MPLC on silica gel (DCM/MeOH, 9:1-8:1) to afford **14** (26 mg, 81%) as colorless oil. $[\alpha]_D^{20}$ +56.1 (*c* 0.3, MeOH); ^{1}H NMR (500 MHz, $CDCl_3$): δ = 8.25-8.15 (m, 2H, Ar-H), 7.75-7.65 (m, 2H, Ar-H), 7.60-7.55 (m, 2H, Ar-H), 7.20-7.17 (m, 2H, Ar-H), 5.64-5.55 (m, 2H, H-1, H-3), 5.49 (dd, *J* = 1.7, 3.3 Hz, 1H, H-2), 5.40 (t, *J* = 10.1 Hz, 1H, H-4), 4.31 (dd, *J* = 5.3, 12.4 Hz, 1H, H-6a), 4.17-4.06 (m, 2H, H-5, H-6b), 2.22, 2.07, 2.06, 2.05 (4 s, 12H, 4 $COCH_3$); ^{13}C NMR (126 MHz, $CDCl_3$): δ = 170.67, 170.14, 170.11, 169.81 (4 CO), 155.61, 128.36, 127.84, 127.49, 116.93 (Ar-C), 95.78 (C-1), 69.36 (C-5), 69.26 (C-2), 68.90 (C-3), 65.89 (C-4), 62.12 (C-6),

20.92, 20.76, 20.73 (4 CO*C*H$_3$); ESI-MS: *m/z*: Calcd for $C_{27}H_{28}N_4NaO_{10}$ $[M+Na]^+$: 591.2, found: 591.1.

5-(4'-(α-D-Mannopyranosyloxy)-biphenyl-4-yl)-1*H*-tetrazole (10h). Prepared according to the procedure described for **10e** from **14** (26 mg, 0.03 mmol). Yield: 18 mg (quant.) as a white solid. $[\alpha]_D^{20}$ +112.1 (*c* 0.1, MeOH/H_2O, 2:1); ^{1}H NMR (500 MHz, CD_3OD): δ = 7.98-7.96 (m, 2H, Ar-H), 7.72-7.71 (m, 2H, Ar-H), 7.58-7.54 (m, 2H, Ar-H), 7.16-7.13 (m, 2H, Ar-H), 5.46 (d, *J* = 1.7 Hz, 1H, H-1), 3.94 (dd, *J* = 1.9, 3.5 Hz, 1H, H-2), 3.83 (dd, *J* = 3.4, 9.5 Hz, 1H, H-3), 3.68-3.61 (m, 3H, H-4, H-6a, H-6b), 3.52 (ddd, *J* = 2.5, 5.4, 9.7 Hz, 1H, H-5); ^{13}C NMR (126 MHz, CD_3OD): δ = 158.19, 145.07, 134.97, 129.29, 128.74, 128.55, 118.26 (Ar-C), 100.13 (C-1), 75.52 (C-5), 72.42 (C-3), 71.98 (C-2), 68.33 (C-4), 62.69 (C-6); HRMS: *m/z*: Calcd for $C_{19}H_{21}N_4O_6$ $[M+H]^+$: 401.1456, found: 401.1450.

4'-(2,3,4,6-Tetra-*O*-acetyl-α-D-mannopyranosyloxy)-3'-chloro-biphenyl-4-carbonitrile (19). Prepared according to the procedure described for **13e** from aryl iodide **18**[23] (79 mg, 0.135 mmol), **12g** (22 mg, 0.15 mmol), Pd(dppf)Cl_2·CH_2Cl_2 (3.3 mg, 4 μmol) and K_3PO_4 (57 mg, 0.27 mmol). Yield: 57 mg (75%) as a white solid. $[\alpha]_D^{20}$ +77.7 (*c* 0.5, $CHCl_3$); ^{1}H NMR (500 MHz, $CDCl_3$): δ = 7.72 (d, *J* = 8.3 Hz, 2H, Ar-H), 7.63 (m, 3H, Ar-H), 7.43 (dd, *J* = 2.2, 8.6 Hz, 1H, Ar-H), 7.27 (d, *J* = 8.6 Hz, 1H, Ar-H), 5.64-5.59 (m, 2H, H-1, H-2), 5.54 (dd, *J* = 1.9, 3.2 Hz, 1H, H-3), 5.41 (t, *J* = 10.1 Hz, 1H, H-4), 4.28 (dd, *J* = 5.2, 12.3 Hz, 1H, H-6a), 4.17 (ddd, *J* = 2.1, 5.1, 10.0 Hz, 1H, H-5), 4.10 (dd, *J* = 2.2, 12.3 Hz, 1H, H-6b), 2.21 (s, 3H, $COCH_3$), 2.12- 2.00 (m, 9H, 3 $COCH_3$); ^{13}C NMR (126 MHz, $CDCl_3$): δ = 170.54, 170.08, 169.90, 169.84, (4C, CO) 151.67, 143.61, 135.29, 132.87, 129.41, 127.53, 126.60, 125.20, 118.79, 117.36, 111.47 (Ar-C, CN), 96.72 (C-1), 70.00 (C-5), 69.39 (C-3), 68.82 (C-2), 65.86

(C-4), 62.16 (C-6), 20.98, 20.81, 20.79, 20.78 (4 CO*C*H_3); ESI-MS*: m/z*: Calcd for $C_{27}H_{26}ClNNaO_{10}$ $[M+Na]^+$: 582.1, found: 582.1.

3'-Chloro-4'-(α-D-mannopyranosyloxy)-biphenyl-4-carbonitrile (10j). Prepared according to the procedure described for **10e** from **19** (36 mg, 0.06 mmol). Yield: 12 mg (48%) as a white solid. $[\alpha]_D^{20}$ +109.4 (*c* 0.23, MeOH); ^{1}H NMR (500 MHz, CD_3OD): δ = 7.80-7.72 (m, 5H, Ar-H), 7.59 (dd, *J* = 2.2, 8.6 Hz, 1H, Ar-H), 7.48 (d, *J* = 8.7 Hz, 1H, Ar-H), 5.62 (d, *J* = 1.4 Hz, 1H, H-1), 4.12 (dd, *J* = 1.8, 3.3 Hz, 1H, H-2), 4.00 (dd, *J* = 3.4, 9.5 Hz, 1H, H-3), 3.83-3.68 (m, 3H, H-4, H-6a, H-6b), 3.63 (ddd, *J* = 2.3, 5.4, 9.6 Hz, 1H, H-5); ^{13}C NMR (126 MHz, CD_3OD): δ = 153.65, 145.15, 135.42, 133.86, 129.82, 128.53, 127.87, 125.47, 119.70, 118.59 (Ar-C), 111.97 (CN), 100.66 (C-1), 76.05 (C-5), 72.39 (C-3), 71.80 (C-2), 68.20 (C-4), 62.65 (C-6); IR (KBr), ν = 3400 (OH), 2227 (C≡N), 1606, 1487 (Ar-C=C) cm^{-1}; HRMS: *m/z*: Calcd for $C_{19}H_{18}ClNNaO_6$ $[M+Na]^+$: 414.0715, found: 414.0721.

3'-Chloro-*N*-(3',6'-dihydroxy-3-oxo-3*H*-spiro[isobenzofuran-1,9'-xanthen]-5-yl)-4'-(α-D-mannopyranosyloxy)-biphenyl-4-carboxamide (22). Compound **21** (10.0 mg, 0.024 mmol), fluoresceinamine isomer I (12.7 mg, 0.037 mmol) and COMU (20.9 mg, 0.049 mmol) were dissolved in dry DMF (1 mL), then NEt_3 (10 µL, 0.073 mmol) was added and the mixture was stirred at rt for 7 h. 1 N HCl in DMF was added until acid reaction on pH paper and the mixture was concentrated. The residue was dissolved in DCM/MeOH (3:1) and loaded onto a silica gel column. The complex mixture of compounds was only partially resolved. The fractions containing the product were collected, concentrated and purified by preparative HPLC (gradient H_2O/MeCN, +0.2% HCO_2H), to afford compound **22** (5 mg, 19%). $[\alpha]_D^{20}$ +21.1 (*c* 0.10, MeOH); ^{1}H NMR (500 MHz, CD_3OD): δ = 8.26 (d, *J* = 8.4 Hz, 2H, Ar-H), 7.88-7.74 (m, 3H, Ar-H), 7.66 (dd, *J* = 2.2, 8.6 Hz, 1H, Ar-H), 7.51 (d, *J* = 8.7 Hz, 1H, Ar-H),

7.29 (dd, *J* = 1.9, 5.3 Hz, 2H, Ar-H), 7.19 (dd, *J* = 2.1, 8.3 Hz, 1H, Ar-H), 7.08-6.99 (m, 2H, Ar-H), 6.95 (d, *J* = 8.7 Hz, 1H, Ar-H), 6.72 (dd, *J* = 5.5, 10.6, Hz, 2H, Ar-H), 6.61 (dd, *J* = 2.3, 8.7 Hz, 1H, Ar-H), 5.65 (s, 1H, H-1), 4.15 (dd, *J* = 1.8, 3.2 Hz, H-2), 4.03 (dd, *J* = 3.4, 9.5, Hz, H-3), 3.87-3.72 (m, 3H, H-4, H-6a, H-6b), 3.65 (m, 1H, H-5); ^{13}C NMR (126 MHz, CD_3OD): δ = 137.50, 136.01, 131.90, 130.24, 130.20, 129.87, 129.24, 128.03, 127.91, 125.79, 125.46, 124.73, 118.99, 118.76, 118.65 (Ar-C), 100.73 (C-1), 76.06 (C-5), 72.42 (C-3), 71.85 (C-2), 68.24 (C-4), 62.69 (C-2); ESI-MS: *m/z*: Calcd for $C_{39}H_{31}ClNO_{12}$ $[M+H]^+$: 740.2, found: 740.2.

3'-Chloro-*N*-(2-(3-(3',6'-dihydroxy-3-oxo-3*H*-spiro[isobenzofuran-1,9'-xanthen]-5-yl)-thioureido)ethyl)-4'-(α-D-mannopyranosyloxy)-biphenyl-4-carboxamide (23). To a stirred solution of compound **21** (25 mg, 0.061 mmol) in dry DMF (1 mL), NHS (21 mg, 0.183 mmol) was added, followed by DIC (9.2 mg, 0.073 mmol). The mixture was stirred at rt for 2 h, then *N*-Boc-ethylendiamine (10.7 mg, 0.067 mmol) was added and the reaction was stirred for 10 h. It was then cooled down to 0 °C, diluted with water and concentrated. Chromatography on silica gel (DCM/MeOH) yielded 23 mg (0.042 mmol, 68%) of *tert*-butyl (3'-chloro-4'-(α-D-mannopyranosyloxy)-biphenyl-4-yl-carboxamido)ethyl)carbamate. This product was dissolved in DCM (3 mL) and TFA (1 mL) was added. The solid dissolved during addition of TFA. After 10 min the reaction was complete. The mixture was evaporated and excess TFA was removed in high vacuum. The intermediate *N*-(2-aminoethyl)-3'-chloro-4'-(α-D-manno-pyranosyloxy)-biphenyl-4-carboxamide TFA salt (23 mg, 0.042 mmol, quant.) was used directly in the next step. It was dissolved in dry DMF (0.5 mL) and NEt_3 (12.8 mg, 0.127 mmol) was added. The mixture was cooled to 0 °C, then FITC (14.8 mg, 0.038 mmol) was added and the mixture was stirred for 3 h in the dark. The mixture was then co-evaporated with water, taken up in MeOH/10% aq. acetic acid and evaporated. Chromatography on silica gel (DCM/MeOH) yielded compound **23**, contaminated with triethylammonium acetate. The

compound was then re-dissolved in MeOH, and 0.5 N HCl in MeOH was added. The mixture was evaporated and chromatographed on silica gel, to yield pure **23** (15 mg, 47%). $[\alpha]_D^{20}$ +12.1 (*c* 0.30, MeOH); ^{1}H NMR (500 MHz, CD_3OD): δ = 8.12 (s, 1H), 7.92 (d, *J* = 8.3 Hz, 2H, Ar-H), 7.70 (dd, *J* = 5.0, 13.1 Hz, 2H, Ar-H), 7.64 (d, *J* = 8.3 Hz, 2H, Ar-H), 7.54 (dd, *J* = 2.2, 8.6 Hz, 1H, Ar-H), 7.46 (d, *J* = 8.7 Hz, 1H, Ar-H), 7.09 (d, *J* = 8.2 Hz, 1H, Ar-H), 6.74 (s, 2H), 6.69 (d, *J* = 1.4 Hz, 2H, Ar-H), 6.55 (d, *J* = 8.4 Hz, 2H, Ar-H), 5.63 (d, *J* = 1.3 Hz, H-1), 4.15 (dd, *J* = 1.8, 3.1 Hz, H-2), 4.03 (dd, *J* = 3.4, 9.5 Hz, H-3), 3.94 (s, 2H, CH_2), 3.86-3.64 (m, 6H, H-4, H-5, H-6, CH_2); ^{13}C NMR (126 MHz, CD_3OD): δ = 153.21, 143.84, 136.41, 129.66, 129.18, 127.76, 127.70, 125.37, 118.64, 103.62 (Ar-C), 100.75 (C-1), 76.00 (C-5), 72.41 (C-3), 71.86 (C-2), 68.24 (C-4), 62.69 (C-6), 40.76 (CH_2); ESI-MS: *m/z*: Calcd for $C_{42}H_{37}ClN_3O_{12}S$ $[M+H]^+$: 842.2, found: 842.2.

3'-Chloro-*N*-(2-(2-(2-(3-(3',6'-dihydroxy-3-oxo-3*H*-spiro[isobenzofuran-1,9'-xanthen]-5-yl)thioureido)ethoxy)ethoxy)ethyl)-4'-(α-D-mannopyranosyloxy)-biphenyl-4-carboxamide (24). Compound **21** (280 mg, 0.68 mmol) was dissolved in dry DMF (5 mL) under argon, then NHS (235 mg, 2.04 mmol) was added, followed by DIC (0.12 mL, 0.78 mmol) and the mixture was stirred at rt for 4 h, then Boc-PEG2-NH_2 (186 mg, 0.75 mmol) was added, and the mixture was stirred at rt under argon for 10 h. It was then slowly diluted with water and concentrated. The residue was purified by chromatography on silica gel (DCM/MeOH) to give *tert*-butyl (2-(2-(2-(3'-chloro-4'-(α-D-mannopyranosyloxy)-biphenyl-4-ylcarboxamido)ethoxy)ethoxy)ethyl)carbamate (300 mg, 0.468 mmol, 69%). Then, the carbamate was suspended in DCM (3 mL) and TFA (1 mL) was added dropwise at rt. After 30 min, the solvents were evaporated and the crude mixture was dissolved in $CHCl_3$/MeOH (6:4, + 0.5% conc. NH_4OH) and transferred to a silica gel column, eluting with the same solvent mixture, to yield *N*-(2-(2-(2-aminoethoxy)ethoxy)ethyl)-3'-chloro-4'-(α-D-mannopyranosyl-

oxy)-biphenyl-4-carboxamide (228 mg, 90 %). A fraction of the amine (10 mg, 0.018 mmol) was dissolved in dry DMF (0.5 mL) and cooled to 0 °C. FITC (6.5 mg, 0.017 mmol) was added and the mixture was stirred for 1 h. The mixture was concentrated and the residue was purified by chromatography on silica (DCM/MeOH), to yield **24** (10 mg, 65%). ^{1}H NMR (500 MHz, CD_3OD): δ = 8.21 (d, *J* = 1.4 Hz, 1H, Ar-H), 7.88 (d, *J* = 8.3 Hz, 2H, Ar-H), 7.68 (d, *J* = 2.2 Hz, 2H, Ar-H), 7.63 (d, *J* = 8.3 Hz, 2H, Ar-H), 7.53 (dd, *J* = 2.2, 8.6 Hz, 1H, Ar-H), 7.43 (d, *J* = 8.7 Hz, 1H, Ar-H), 7.09 (d, *J* = 8.2 Hz, 1H, Ar-H), 6.68 (d, *J* = 2.3 Hz, 2H, Ar-H), 6.65 (dd, *J* = 2.6, 8.6 Hz, 2H, Ar-H), 6.53 (dd, *J* = 1.6, 8.7 Hz, 2H, Ar-H), 5.61 (d, *J* = 1.3 Hz, 1H, H-1), 4.14 (dd, *J* = 1.8, 3.2, Hz, 1H, H-2), 4.03 (dd, *J* = 3.4, 9.5 Hz, 1H, H-3), 3.93-3.53 (m, 16H), 3.37 (s, 2H, NCH_2), 1.30 (s, 2H, CH_2); ^{13}C NMR (126 MHz, CD_3OD): δ = 170.01 (CO), 153.17, 143.72, 136.37, 134.37, 130.39, 129.69, 129.04, 127.78, 127.73, 125.35, 118.60, 103.60 (Ar-C), 100.72 (C-1), 75.97 (C-5), 72.41 (C-3), 71.86, 71.40, 70.59 (5C, C-2, OCH_2), 68.23 (C-4), 62.64 (C-6), 49.88, 45.49, 40.97 (CH_2); ESI-MS: *m/z*: Calcd for $C_{46}H_{45}ClN_3O_{14}S$ $[M+H]^+$: 930.2, found: 930.4.

Competitive Fluorescence Polarization Assay

Expression and purification of CRD of FimH. A recombinant protein consisting of the CRD of FimH linked to a 6His-tag via a thrombin cleavage site (FimH-CRD-Th-His_6) was expressed in *E. coli* strain HM125 and purified by affinity chromatography as previously described.[43]

***K*$_D$ determination of FITC-labeled ligands.** The functionalized ligands (**23**, **24**) were prepared as a 10 mM stock solution in pure DMSO (Sigma Aldrich, Buchs, Switzerland). All further dilutions of compounds and FimH-CRD-Th-His_6 protein were prepared in assay buffer (20 mM HEPES, 150 mM NaCl, 50 µg/mL BSA, pH 7.4). BSA was added to the assay buffer

to prevent non-specific binding of protein to the plastic surface. Binding isotherms for the fluorescent ligands were obtained in direct binding studies by adding a constant concentration of ligand (final concentration 5 nM) and a linear dilution of protein (final concentration 0-100 nM) to a final volume of 200 µL in 96-well, black, flat bottom NBS™ plates (Corning Inc., Corning, NY, USA). After incubating the plate for 24 h at rt with gentle shaking, the fluorescence polarization was measured with the Synergy™ H1 Hybrid Multi-Mode Microplate Reader (BioTek Instruments Inc., Winooski, VT, USA) with polarized excitation at 485 nm and emission measured at 528 nm through polarizing filters parallel and perpendicularly oriented to the incident polarized light. K_D values were determined by plotting the FP readout as a function of the protein concentration and applying the following single-site binding equation (Equation 1) that accounts for ligand depletion:

$$S_{obs} = S_F + (S_B - S_F) \times \left(\frac{C_P + C_L + K_D - \sqrt{(C_P + C_L + K_D)^2 - 4C_P C_L}}{2C_L}\right) \quad (1)$$

where S_{obs} is the observed signal from the ligand, S_F is the signal from free ligand, S_B is the signal from bound ligand, C_P is the total concentration of protein, and C_L is the total concentration of ligand.[49]

***K*D Determination of FimH Antagonists.** The fluorescently labeled ligand **23** was used for the competitive fluorescence polarization assay. A linear dilution of non-labeled FimH antagonist with final concentrations ranging from 0-10 µM was titrated into 96-well, black, flat bottom NBS™ plates (Corning Inc.) to a final volume of 200 µL containing a constant concentration of protein (final concentration 25 nM) and FITC-labeled ligand which was fixed at a higher concentration in competitive binding assays than in direct binding experiments to obtain higher fluorescence intensities (final concentration 20 nM). Prior to measuring the fluorescence polarization, the plates were incubated on a shaker for 24 h at rt until the reaction reached equilibrium. The IC_{50} value was determined with Prism (GraphPad Software Inc., La

Jolla, CA, USA) by applying a standard four-parameter IC_{50} function. The obtained IC_{50} values were converted into their corresponding K_D values using the derivation of the Cheng-Prusoff equation.[45] This variation of the Cheng-Prusoff equation is applied to competition assays with tight-binding inhibitors, and includes terms to correct for ligand depletion effects. However, the K_D for antagonists having a higher affinity towards FimH than the labeled ligand could not be accurately determined.[45]

Isothermal Titration Calorimetry (ITC)

All ITC experiments were performed with the FimH-CRD-Th-His_6 protein using a VP-ITC instrument from MicroCal, Inc. (Malvern Instruments, Worcestershire, UK) with a sample cell volume of 1.4523 mL. The measurements were performed with 0 to 5% DMSO at 25 °C, a stirring speed of 307 rpm, and 10 µcal s^{-1} reference power. The protein samples were dialyzed in assay buffer prior to all experiments. Due to the high protein consumption of ITC, only the experiments for the reference compounds (**1, 3** and **25**) were measured in duplicates. Compounds **1, 3**, **9**, and **25** were measured in a direct fashion by titration of ligand (100-2,000 µM) into protein (8.6-55 µM) with injections of 3-8 µL at intervals of 10 min to ensure non-overlapping peaks. The quantity $c = Mt(0)\ K_D^{-1}$, where $Mt(0)$ is the initial macromolecule concentration, is of importance in titration microcalorimetry. The *c*-values of the direct titrations were below 1,000 and thus within the reliable range. For the compounds **10b-e, 10g** and **10j** additional competitive ITC experiments were performed due to their high affinity resulting in *c*-values above 1,000 for direct titrations. These ligands (600 µM) were titrated into protein (30 µM), which was preincubated with compound **25** (300 µM) resulting in sigmoidal titration curves. Due to slow reaction kinetics, titration intervals of 20 min were used.

Baseline correction and peak integration was performed using the Origin 7 software (OriginLab, Northampton, MA, USA). An initial 2 µL injection was excluded from data analysis. Baseline subtraction and curve-fitting with the three variables *N* (concentration correction factor), K_D (dissociation constant), and $\Delta H°$ (change in enthalpy) was performed with the SEDPHAT software version 10.40 (National Institute of Health).[86] A global fitting analysis was performed for the competition titration (compounds **10b-e**, **10g** or **10j** competing for the protein binding site with compound **25**) and the direct titration of the competitor (compound **25** binding to protein) to fit for K_D. $\Delta H°$ and *N* were fitted from direct titrations of compounds **10b-e**, **10g** or **10j** into protein. For the compounds **3, 9** and **25** binding to protein all variables could be determined from a global analysis of the direct titration.

The thermodynamic parameters were calculated with the following equation (Equation 2):

$$\Delta G° = \Delta H° - T\Delta S° = RT \ln K_D = -RT \ln K_A \quad (2)$$

where $\Delta G°$, $\Delta H°$, and $\Delta S°$ are the changes in free energy, enthalpy, and entropy of binding, respectively, *T* is the absolute temperature, and *R* is the universal gas constant (8.314 J mol^{-1} K^{-1}). The 95 %-confidence intervals of the measurements were calculated for the two variables K_D and $\Delta H°$ with the 1-dimensional error surface projection within the SEDPHAT software.

Calculation of the Free Energy of Desolvation. The three dimensional representation for each of the aglycons (4-methoxy biphenyl scaffold, Figure 7) was built in the Maestro[87] modeling environment and the global minimum conformation was identified by performing 500 iterations of the mixed torsional/low-mode conformational sampling in combination with the OPLS-2005 force-field and the implicit solvent model (water) as implemented in the Macromodel 9.9.[88] The global minimum structures were used as input for the AMSOL 7.1 program[89] to obtain the free energy of desolvation ΔG_{des} (Table 5) with the SM5.4A solvation

model[90] and the AM1[91] level of theory (used keywords "AM1 SM5.4A SOLVNT=WATER TRUES").

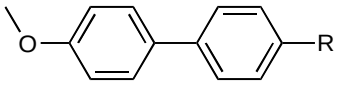

Figure 7. The 4-methoxy biphenyl scaffold of aglycons.

Table 5. Aqueous free energy of desolvation.

R	**ΔG_{des} [kJ/mol]**
neutral	
H	15.6
$CONHCH_3$	39.9
$COOCH_3$	23.0
SO_2NHCH_3	65.5
SO_2CH_3	56.4
4-morpholine amide	45.3
CN	22.0
deprotonated	
COO^-	298.2
SO_2-N^--Me	342.0

Determination of the MAC_{90} by flow cytometry

The MAC_{90} was determined in principle as in the previously published flow cytometry assay,[79] but with some modifications. The human epithelial bladder carcinoma cell line 5637 (DSMZ,

Braunschweig, Germany) was grown in RPMI 1640 medium, supplemented with 10% fetal calf serum (FCS), 100 U/mL penicillin and 100 µg/mL streptomycin at 37 °C, 5% CO_2. All solutions were purchased from Invitrogen (Basel, Switzerland). The cells were subcultured 1:6 twice per week [using Trypsin/EDTA (Sigma-Aldrich) for the detachment]. Two days before infection, 1.8×10^5 cells were seeded in each well of a 24-well plate in RPMI 1640 containing 10% FCS without antibiotics. The cell density was approximately $3\text{-}5 \times 10^5$ cells/well at the assay day.

For infection, the GFP-expressing clinical *E. coli* isolate UTI89[92] (UTI89 wt) and the GFP-expressing FimA-H knock-out strain UTI89 Δ*fimA-H* were used (strains were provided by Prof. Urs Jenal, Biocenter, University of Basel, Switzerland).[79] Bacteria were cultivated at 37 °C in 10 mL Luria-Bertani (LB) broth (Becton, Dickinson and Company) overnight, harvested by centrifugation (3,800 rpm, 10 min) and washed three times in phosphate buffered saline (PBS, Sigma-Aldrich) and a bacterial solution of OD_{600} of 0.75 in RPMI + 10% FCS was prepared. For the determination of the MAC_{90} value, the IC_{90}, linear dilutions of the FimH-antagonist were prepared in 5% DMSO and PBS. Bacteria and antagonists were pre-incubated for 10 min at 37 °C, before cells were infected with either only 200 µL bacterial solution of UTI89 or UTI89 Δ*fimA-H* (positive and negative controls), or 225 µL of the pre-incubated bacteria-antagonist mixture. Infection lasted for 1.5 h, during this time infected cells were incubated at 37 °C. Then, cells were washed with PBS and detached from wells by the addition of 150 µL trypsin and incubation at 37 °C for 10 min, before flushing from wells PBS containing 2% FCS and transferred to tubes. To dilute the trypsin, cells were centrifuged at 13000 rpm, 1 min, 600 µL of the supernatant was discarded and the pellet was re-suspended in the remaining 300 µL PBS containing 2% FCS. Samples were stored on ice until measurement. Before analysis with the flow cytometer (Becton Dickinson, FACSCanto II), the

samples were gently mixed and filtered using a 35 µm nylon mesh (Corning Life Sciences) to prevent cellular aggregation. Cells were gated with linear scaling for side scatter (SSC) and forward scatter (FSC) and GFP intensity of live cells was evaluated. IC_{90} values were determined by plotting the concentration of the antagonist in a logarithmic mode versus the mean fluorescence intensity (MFI) of living cells and by fitting a dose response curve (variable slope, four parameters) with the prism software (GraphPad Prism).

X-ray analysis of the antagonists 10e and 10j co-crystallized with FimH-CRD

FimH-CRD-10e co-crystallization. Initial FimH-CRD (18 mg/mL in 20 mM HEPES pH 7.4) crystals were obtained in complex with 4-(5-nitroindolin-1-yl)phenyl α-D-mannopyranoside (5 mM).[23] Crystals were grown in sitting-drop vapor diffusion at 20 °C with 200 nL of protein-antagonist mixture together with 200 nL precipitant solution in well D3 (0.2 M sodium phosphate monobasic monohydrate, 20% w/v PEG 3,350) of the PEG/Ion HT™ screen (Hampton Research, CA, USA). Cubic crystals appeared within one week, which served as cross-seeding crystals. A solution of FimH-CRD (20 mg/mL) and **10e** (5 mM) was mixed with 0.2 M sodium phosphate monobasic monohydrate, 20% w/v PEG 400 with 0.5 µL of each solution. Streak-seeding was performed after one day of incubation. Cubic FimH-CRD-**10e** crystals formed within 24 h. Crystals were flash cooled to 100 K with perfluoropolyether cryo oil (Hampton Research, CA, USA) as cryoprotectant. Data was collected with synchrotron radiation (λ = 0.99999 Å) at the PXIII beamline, Swiss Light Source, Switzerland.

FimH-CRD-10j co-crystallization. Co-crystals were initially grown in sitting-drop vapor diffusion at 20 °C with 0.5 µL of a mixture of FimH-CRD (20 mg/mL) and **10j** (5 mM) together with 0.5 µL of 0.1 M HEPES pH 7.5, 2 M ammonium sulfate. Plate-like crystals

formed within two weeks and were used as seeds for subsequent crystallization. Diffraction quality crystals were grown by streak-seeding in 0.5 µL of FimH-CRD (10 mg/mL) with **10j** (2.5 mM) and 0.5 µL of 0.1 M HEPES pH 7.5, 1.25 M ammonium sulfate. The drops were covered with perfluoropolyether cryo oil prior to flash cooling to 100 K. Data was collected with synchrotron radiation (λ = 1.00003 Å) at the PXIII beamline, Swiss Light Source, Switzerland.

Structure Determination and Refinement. Data were indexed and integrated with the XDS package[93] for the FimH-CRD-**10e** co-crystal structure, and with mosflm[94] for the FimH-CRD-**10j** co-crystal structure. Scaling was performed with XDS and SCALA included in the CCP4 suite, respectively.[95] Structures were solved by molecular replacement with PHASER[96] using the FimH-CRD-butyl α-D-mannopyranoside complex (PDB code 1UWF) as search model. The structures were iteratively built using the COOT software[97] and refined with the PHENIX software.[98] Geometric restraints for **10e** and **10j** were generated with PRODRG.[99] The models were validated using molprobity.[100] Residues 113-115 were not modeled in the **10e** structure due to disorder. Furthermore, the ligand was modeled in two possible conformations. For both ligands, electron density is reduced on the second aromatic ring due to flexibility of the ligand.

Table 6. Data Collection and Refinement Statistics for FimH-CRD-**10e** and FimH-CRD-**10j** co-crystals.

	FimH-CRD-**10e**	FimH-CRD-**10j**
PDB code	4CSS	4CST
Space group	P 2_1 2_1 2_1	P 2_1 2_1 2_1
No. of molecules in the asymmetric unit	1	1
Cell dimensions		
a, *b*, *c* (Å)	48.38, 56.23, 61.59	48.84, 55.89, 61.00

□□□□ *a, b, c* (°)	90, 90, 90	90, 90, 90
Data Collection		
Beamline	Swiss Light Source PXIII	Swiss Light Source PXIII
Resolution range (Å)[a]	30.0 - 1.07 (1.13 – 1.07)	23.5 – 1.10 (1.12 – 1.10)
Unique observations[a]	72000 (9354)	66470 (2500)
Average multiplicity[a]	10.9 (3.7)	5.4 (2.4)
Completeness (%)	96.1 (78.0)	97.2 (76.5)
R_{merge}[a]	0.056 (0.57)	0.051 (0.305)
Mean I / σ(I)[a]	21.5 (2.22)	15.5 (2.9)
Refinement		
Resolution range (Å)	15.7 – 1.07	23.5 – 1.10
R, R_{free}	11.2, 13.2	11.4, 13.0
Rms deviation from ideal bond length (Å)	0.010	0.010
Rms deviation from ideal bond angle (deg)	1.170	1.420

[a]Values in parentheses are for highest-resolution shell.

Physicochemical and *in vitro* pharmacokinetic studies.

Materials. Dimethyl sulfoxide (DMSO), 1-propanol, 1-octanol, Dulbecco's Modified Eagle's Medium (DMEM) - high glucose, L-glutamine solution, penicillin-streptomycin solution, Dulbecco's Phosphate Buffered Saline (DPBS), trypsin-EDTA solution, magnesium chloride hexahydrate, and reduced nicotinamide adenine dinucleotide phosphate (NADPH) were purchased from Sigma-Aldrich. MEM nonessential amino acid (MEM-NEAA) solution, fetal bovine serum (FBS), and DMEM without sodium pyruvate and phenol red were bought from

Invitrogen (Carlsbad, CA, USA). PRISMA HT universal buffer, GIT-0 Lipid Solution, and Acceptor Sink Buffer were ordered from pIon (Woburn, MA, USA). Human plasma was bought from Biopredic (Rennes, France) and acetonitrile (MeCN) and methanol (MeOH) from Acros Organics (Geel, Belgium). Pooled male rat liver microsomes were purchased from BD Bioscience (Franklin Lakes, NJ, USA). Tris(hydroxymethyl)-aminomethane (TRIS) was obtained from AppliChem (Darmstadt, Germany). The Caco-2 cells were kindly provided by Prof. G. Imanidis, FHNW, Muttenz, and originated from the American Type Culture Collection (Rockville, MD, USA).

pK_a. The pK_a values were determined as described elsewhere.[101] In brief, the pH of a sample solution was gradually changed and the chemical shift of protons adjacent to ionizable centers was monitored by ^{1}H nuclear magnetic resonance (NMR) spectroscopy. The shift was plotted against the pH of the respective sample, and the pK_a was read out from the inflection point of the resulting sigmoidal curve.

Log $D_{7.4}$. The in silico prediction tool ALOGPS[102] was used to estimate log *P* values of the compounds. Depending on these values, the compounds were classified into three categories: hydrophilic compounds (log *P* below zero), moderately lipophilic compounds (log *P* between zero and one) and lipophilic compounds (log *P* above one). For each category, two different ratios (volume of 1-octanol to volume of buffer) were defined as experimental parameters (Table 7).

Table 7. Compound classification based on estimated log *P* values.

Compound type	**log *P***	**ratio (1-octanol / buffer)**
hydrophilic	< 0	30:140, 40:130
moderately lipophilic	0 - 1	70:110, 110:70

lipophilic	> 1	3:180, 4:180

Equal amounts of phosphate buffer (0.1 M, pH 7.4) and 1-octanol were mixed and shaken vigorously for 5 min to saturate the phases. The mixture was left until separation of the two phases occurred, and the buffer was retrieved. Stock solutions of the test compounds were diluted with buffer to a concentration of 1 µM. For each compound, six determinations, that is, three determinations per 1-octanol/buffer ratio, were performed in different wells of a 96-well plate. The respective volumes of buffer containing analyte (1 µM) were pipetted to the wells and covered by saturated 1-octanol according to the chosen volume ratio. The plate was sealed with aluminum foil, shaken (1,350 rpm, 25 °C, 2 h) on a Heidolph Titramax 1000 plate-shaker (Heidolph Instruments GmbH & Co. KG, Schwabach, Germany) and centrifuged (2,000 rpm, 25 °C, 5 min, 5804 R Eppendorf centrifuge, Hamburg, Germany). The aqueous phase was transferred to a 96-well plate for analysis by LC-MS.

The log $D_{7.4}$ coefficient was calculated from the 1-octanol/buffer ratio (o:b), the initial concentration of the analyte in buffer (1 µM), and the concentration of the analyte in buffer (c_B) with Equation 3:

$$\log D_{7.4} = \log\left(\frac{1\,\mu M - c_B}{c_B} \cdot \frac{1}{o:b}\right) \quad (3)$$

Aqueous Solubility. Solubility was determined in a 96-well format using the µSOL Explorer solubility analyzer (pIon, version 3.4.0.5). For each compound, measurements were performed at pH 3.0 and 7.4 in triplicates. For this purpose, six wells of a deep well plate, that is, three wells per pH value, were filled with 300 µL of PRISMA HT universal buffer, adjusted to pH 3.0 or 7.4 by adding the requested amount of NaOH (0.5 M). Aliquots (3 µL) of a compound stock solution (10-50 mM in DMSO) were added and thoroughly mixed. The final sample

concentration was 0.1-0.5 mM, the residual DMSO concentration was 1.0% (v/v) in the buffer solutions. After 15 h, the solutions were filtrated (0.2 µm 96-well filter plates) using a vacuum to collect manifold (Whatman Ltd., Maidstone, UK) to remove the precipitates. Equal amounts of filtrate and 1-propanol were mixed and transferred to a 96-well plate for UV/Vis detection (190 to 500 nm, SpectraMax 190). The amount of material dissolved was calculated by comparison with UV/Vis spectra obtained from reference samples, which were prepared by dissolving compound stock solution in a 1:1 mixture of buffer and 1-propanol (final concentrations 0.017-0.083 mM).

Parallel Artificial Membrane Permeation Assay (PAMPA). Effective permeability (log P_e) was determined in a 96-well format with the PAMPA.[60] For each compound, measurements were performed at pH 5.0 and 7.4 in quadruplicates. Eight wells of a deep well plate, that is, four wells per pH-value, were filled with 650 µL of PRISMA HT universal buffer adjusted to pH 5.0 or 7.4 by adding the requested amount of NaOH (0.5 M). Samples (150 µL) were withdrawn from each well to determine the blank spectra by UV/Vis-spectroscopy (190 to 500 nm, SpectraMax 190). Then, analyte dissolved in DMSO was added to the remaining buffer to yield 50 µM solutions. To exclude precipitation, the optical density was measured at 650 nm, with 0.01 being the threshold value. Solutions exceeding this threshold were filtrated. Afterwards, samples (150 µL) were withdrawn to determine the reference spectra. Further 200 µL were transferred to each well of the donor plate of the PAMPA sandwich (pIon, P/N 110163). The filter membranes at the bottom of the acceptor plate were infused with 5 µL of GIT-0 Lipid Solution, and 200 µL of Acceptor Sink Buffer was filled into each acceptor well. The sandwich was assembled, placed in the GutBox™, and left undisturbed for 16 h. Then, it was disassembled and samples (150 µL) were transferred from each donor and acceptor well to UV-plates for determination of the UV/Vis spectra. Effective permeability (log P_e) was calculated from the compound flux deduced from the spectra, the filter area, and the initial

sample concentration in the donor well with the aid of the PAMPA Explorer Software (pIon, version 3.5).

Colorectal Adenocarcinoma (*Caco*-2) Cell Permeation Assay. Caco-2 cells were cultivated in tissue culture flasks (BD Biosciences) with DMEM high glucose medium, containing L-glutamine (2 mM), nonessential amino acids (0.1 mM), penicillin (100 U/mL), streptomycin (100 µg/mL), and fetal bovine serum (10%). The cells were kept at 37 °C in humidified air containing 5% CO_2, and the medium was changed every second day. When approximately 90% confluence was reached, the cells were split in a 1:10 ratio and distributed to new tissue culture flasks. At passage numbers between 60 and 65, they were seeded at a density of 5.3×10^5 cells per well to Transwell 6-well plates (Corning Inc.) with 2.5 mL of culture medium in the basolateral and 1.8 mL in the apical compartment. The medium was renewed on alternate days. Permeation experiments were performed between days 19 and 21 post seeding. Prior to the experiment, the integrity of the Caco-2 monolayers was evaluated by measuring the transepithelial electrical resistance (TEER) with an Endohm tissue resistance instrument (World Precision Instruments Inc., Sarasota, FL, USA). Only wells with TEER values higher than 250 Ω cm^2 were used. Experiments were performed in the apical-to-basolateral (absorptive) and basolateral-to-apical (secretory) directions in triplicates. Transport medium (DMEM without sodium pyruvate and phenol red) was withdrawn from the donor compartments of three wells and replaced by the same volume of compound stock solution (10 mM in DMSO) to reach an initial sample concentration of 62.5 µM. The Transwell plate was then shaken (600 rpm, 37 °C) on a Heidolph Titramax 1000 plate-shaker. Samples (40 µL) were withdrawn from the donor and acceptor compartments 30 min after initiation of the experiment and the compound concentrations were determined by LC-MS (see below). Apparent permeability (P_{app}) was calculated according to Equation 4:

$$P_{app} = \frac{dQ}{dt} \times \frac{1}{A \times c_0} \quad (4)$$

where dQ/dt is the compound flux (mol s^{-1}), A is the surface area of the monolayer (cm^2), and c_0 is the initial concentration in the donor compartment (mol cm^{-3}).[60] After the experiment, TEER values were assessed again for each well and results from wells with values below 250 Ω cm^2 were discarded.

Plasma Protein Binding (PPB). PPB was determined in a 96-well format using a high throughput dialysis block (HTD96b; HTDialysis LCC, Gales Ferry, CT, USA). For each compound, measurements were performed in triplicate. Dialysis membranes (MWCO 12-14 K; HTDialysis LCC) were hydrated according to the instructions of the manufacturer and placed into the dialysis block. Human plasma was centrifuged (5,800 rpm, 5 °C, 10 min), the pH of the supernatant (without floating plasma lipids) was adjusted to 7.4 by adding the requested amount of HCl (4 M), and analyte was added to yield a final concentration of 10 µM. Equal volumes (150 µL) of plasma containing the analyte or TRIS-HCl buffer (0.1 M, pH 7.4) were transferred to the compartments separated by the dialysis membrane. The block was covered with a sealing film and left undisturbed (5 h, 37 °C). Afterwards, samples (90 µL) were withdrawn from the buffer compartments and diluted with plasma (10 µL). From the plasma compartments, samples (10 µL) were withdrawn and diluted with TRIS-HCl buffer (90 µL). The solutions were further diluted with ice-cooled MeCN (300 µL) to precipitate the proteins and centrifuged (3600 rpm, 4 °C, 10 min). The supernatants (50 µL) were retrieved, and the analyte concentrations were determined by LC-MS (see below). The fraction bound (f_b) was calculated as follows (Equation 5):

$$f_b = 1 - \frac{c_b}{c_p} \quad (5)$$

where c_b is the concentration of the analyte withdrawn from the buffer compartment before dilution and c_p is the concentration in the plasma compartment. The values were accepted if the recovery of analyte was between 80 and 120% of the initial amount.

Cytochrome P450-mediated metabolism. Incubations consisted of pooled male rat liver microsomes (0.5 mg microsomal protein/mL), test compound (2 µM), $MgCl_2$ (2 mM), and NADPH (1 mM) in a total volume of 300 µL TRIS-HCl buffer (0.1 M, pH 7.4) and were performed in a 96-well plate on a Thermomixer Comfort (Eppendorf). Compounds and microsomes were preincubated (37 °C, 700 rpm, 10 min) before NADPH was added. Samples (50 µL) at t = 0 min and after an incubation time of 5, 10, 20, and 30 min were quenched with 150 µL of ice-cooled MeOH, centrifuged (3,600 rpm, 4 °C, 10 min), and 80 µL of supernatant was transferred to a 96-well plate for LC-MS analysis (see below). The metabolic half-life ($t_{1/2}$) was calculated from the slope of the linear regression from the log percentage remaining compound versus incubation time relationship. Control experiments without NADPH were performed in parallel.

LC-MS measurements. Analyses were performed using an 1100/1200 Series HPLC System coupled to a 6410 Triple Quadrupole mass detector (Agilent Technologies, Inc., Santa Clara, CA, USA) equipped with electrospray ionization. The system was controlled with the Agilent MassHunter Workstation Data Acquisition software (version B.01.04). The column used was an Atlantis® T3 C18 column (2.1 × 50 mm) with a 3 µm particle size (Waters Corp., Milford, MA, USA). The mobile phase consisted of eluent A: H_2O containing 0.1% formic acid (for **10a-f**, **h-i**), or 10 mM ammonium acetate, pH 5.0 in 95:5, H_2O/MeCN (for **10g**, **j**); and eluent B: MeCN containing 0.1% formic acid. The flow rate was maintained at 0.6 mL/min. The gradient was ramped from 95% A/5% B to 5% A/95% B over 1 min, and then hold at 5%

A/95% B for 0.1 min. The system was then brought back to 95% A/5% B, resulting in a total duration of 4 min. MS parameters such as fragmentor voltage, collision energy, polarity were optimized individually for each analyte, and the molecular ion was followed for each compound in the multiple reaction monitoring mode. The concentrations of the analytes were quantified by the Agilent Mass Hunter Quantitative Analysis software (version B.01.04).

***In Vivo* Studies.**

Animals. Female C3H/HeN mice weighing between 19 and 25 g were obtained from Charles River Laboratories (Sulzfeld, Germany) or Harlan (Venray, Netherlands) and were housed three or four per cage. The mice were kept under specific pathogen-free conditions in the Animal House of the Department of Biomedicine, University Hospital of Basel, and animal experimentation guidelines according to the regulations of the Swiss veterinary law were followed. After 7 d of acclimatization, 9-10 week old mice were used for the studies. Animals had free access to chow and water at any time and were kept in a 12h/12h light/dark cycle. For administration volumes and sampling the good practice guidelines were followed.[101]

Pharmacokinetic studies. The single-dose studies for the first experiment set were performed by intravenous application of FimH antagonists at a dosage of 50 mg/kg body weight, followed by plasma and urine sampling. Antagonists were diluted in PBS (Sigma-Aldrich) for injection into the tail vein. Blood and urine samples (10 µL) were taken at 6 and 30 min, and 1, 2, 4, 6, and 8 h after injection. For the PK studies with **10j**, the antagonist was dissolved in PBS with 5 % DMSO (Sigma-Aldrich) and injected into the tail vain (0.625 mg/kg) or given orally (1.25 mg/kg) using a gavage (syringes from BD Micro Fine, U-100 Insuline, 30 G with BD Microlance 3, 25 G needles, Becton Dickinson and Soft-Ject, 1 mL syringes from Henke Sass Wolf; gavage from Fine Science Tools). Blood and urine were sampled (10 µL) after 7, 13, 20,

30, 45 min, and 1, 1.5, 2, 2.5, 3, 4, 6, 8, and 24 h. Both, blood and urine samples, were directly diluted after sampling with MeOH (Acros Organics) to precipitate the proteins and centrifuged for 11 min at 13,000 rpm. The supernatants were transferred to a 96-well plate (Agilent Technologies, 0.5 mL, polypropylene) and the analyte concentrations were determined by LC-MS (see above).

Infection study. For all infection studies, the drinking water of the mice was replaced by water containing 5% glucose (monohydrate from AppliChem, BioChemica), three days before the start of the experiment. **10j** was dosed at 1.25 mg/kg (in 5% DMSO and PBS) and 10 mg/kg (in 5% DMSO in PBS containing 1% Tween 80, all purchased from Sigma-Aldrich) and applied orally via gavage to 6 and 4 mice, respectively, as described in the pharmacokinetic studies, 40 min prior to infection. Ciprofloxacin (Ciproxin® solution, 2 mg/ml, Bayer) was dosed with 8 mg/kg, which would correspond to a human dose of 500 mg,[81] subcutaneously 10 min prior to infection with UTI89 to 4 mice. The values for the control group (PBS, p.o.) resulted from the infection of 11 mice. Four mice were orally treated with the formulation vehicle for **10j** (5% DMSO in PBS containing 1% Tween 80) and termed controls formulation. Before infection, remaining urine in the bladder was expelled by gentle pressure on the abdomen. Mice were anaesthetized in 2.5 vol% isoflurane/oxygen mixture (Attane, Minrad Inc, USA) and placed on their back. Infection was performed transurethrally using a polyethylene catheter (Intramedic polyethylene tubing, inner diameter 0.28 mm, outer diameter 0.61 mm, Becton Dickinson), on a syringe (Hamilton Gastight Syringe 50 µL, removable 30G needle, BGB Analytik AG, Switzerland). After gentle insertion of the catheter into the bladder, 50 µL of bacterial suspension of UTI89 (5.5×10^9 to 2.25×10^{10} CFU/mL) was slowly injected. This corresponded to approximately 10^7-10^8 CFU per mouse. Mice were killed by CO_2 three hours after inoculation and bladder and kidneys were aseptically removed. Organs

were homogenized in 1 mL PBS using a tissue lyser (Retsch, Germany). Serial dilutions of bladder and kidneys were plated on Levine Eosin Methylene Blue Agar plates (Becton Dickinson) and CFU were counted after overnight incubation at 37 °C.

Authors Information

Corresponding author

*Tel: +41 61 267 15 51. Fax: +41 61 267 15 52. E-mail: beat.ernst@unibas.ch

Author contributions

# These authors contributed equally to the project

Notes

The authors declare no competing financial interest.

Acknowledgement

The authors thank Prof. Dr. med. Radek Skoda, Department of Biomedicine, University Hospital Basel, Switzerland, for giving us access to the animal facility. The financial support by the Swiss National Science Foundation (SNF interdisciplinary grant K-32K1-120904) is gratefully acknowledged.

References

(1) Foxman, B.; Barlow, R.; D'Arcy, H.; Gillespie, B.; Sobel, J. D. Urinary tract infection: self-reported incidence and associated costs. *Ann. Epidemiol.* **2000**, *10*, 509-515.

(2) Ronald, A. The etiology of urinary tract infection: traditional and emerging pathogens. *Am. J. Med.* **2002**, *113 Suppl. 1A*, 14S-19S.

(3) Fihn, S. D. Acute uncomplicated urinary tract infection in women. *N. Engl. J. Med.* **2003**, *349*, 259-266.

(4) Hooton, T. M.; Besser, R.; Foxman, B.; Fritsche, T. R.; Nicolle, L. E. Acute uncomplicated cystitis in an era of increasing antibiotic resistance: a proposed approach to empirical therapy. *Clin. Infect. Dis.* **2004**, *39*, 75-80.

(5) Sanchez, G. V.; Master, R. N.; Karlowsky, J. A.; Bordon, J. M. In vitro antimicrobial resistance of urinary *Escherichia coli* isolates among U. S. outpatients from 2000 to 2010. *Antimicrob. Agents Chemother.* **2012**, *56*, 2181-2183.

(6) Clatworthy, A. E.; Pierson, E.; Hung, D. T. Targeting virulence: a new paradigm for antimicrobial therapy. *Nature Chem. Biol.* **2007**, *3*, 541-548.

(7) Mulvey, M. A.; Schilling, J. D.; Martinez, J. J.; Hultgren, S. J. Bad bugs and beleaguered bladders: interplay between uropathogenic *Escherichia coli* and innate host defenses. *Proc. Natl. Acad. Sci. U S A* **2000**, *97*, 8829-8835.

(8) Schilling, J. D.; Mulvey, M. A.; Hultgren, S. J. Structure and function of *Escherichia coli* type 1 pili: new insight into the pathogenesis of urinary tract infections. *J. Infect. Dis.* **2001**, *183 Suppl. 1*, S36-40.

(9) Wiles, T. J.; Kulesus, R. R.; Mulvey, M. A. Origins and virulence mechanisms of uropathogenic *Escherichia coli*. *Exp. Mol. Pathol.* **2008**, *85*, 11-19.

(10) Capitani, G.; Eidam, O.; Glockshuber, R.; Grütter, M. G. Structural and functional insights into the assembly of type 1 pili from *Escherichia coli*. *Microbes Infect.* **2006**, *8*, 2284-2290.

(11) Le Trong, I.; Aprikian, P.; Kidd, B. A.; Forero-Shelton, M.; Tchesnokova, V.; Rajagopal, P.; Rodriguez, V.; Interlandi, G.; Klevit, R.; Vogel, V.; Stenkamp, R. E.;

Sokurenko, E. V.; Thomas, W. E. Structural basis for mechanical force regulation of the adhesin FimH via finger trap-like β sheet twisting. *Cell* **2010**, *141*, 645-655.

(12) Sharon, N. Carbohydrates as future anti-adhesion drugs for infectious diseases. *Biochim. Biophys. Acta.* **2006**, *1760*, 527-537.

(13) Firon, N.; Itzhak, O.; Sharon, N. Interaction of mannose-containing oligosaccharides with the fimbrial lectin of *Escherichia coli*. *Biochem. Biophys. Res. Commun.* **1982**, *105*, 1426-1432.

(14) Firon, N.; Ofek, I.; Sharon, N. Carbohydrate specificity of the surface lectins of *Escherichia coli*, *Klebsiella pneumoniae*, and *Salmonella typhimurium*. *Carbohydr. Res.* **1983**, *120*, 235-249.

(15) Bouckaert, J.; Berglund, J.; Schembri, M.; De Genst, E.; Cools, L.; Wuhrer, M.; Hung, C.-S.; Pinkner, J.; Slättegard, R.; Zavialov, A.; Choudhury, D.; Langermann, S.; Hultgren, S. J.; Wyns, L.; Klemm, P.; Oscarson, S.; Knight, S. D.; De Greve, H. Receptor binding studies disclose a novel class of high-affinity inhibitors of the *Escherichia coli* FimH adhesin. *Mol. Microbiol.* **2005**, *55*, 441-455.

(16) Firon, N.; Ashkenazi, S.; Mirelman, D.; Ofek, I.; Sharon, N. Aromatic alpha-glycosides of mannose are powerful inhibitors of the adherence of type 1 fimbriated *Escherichia coli* to yeast and intestinal epithelial cells. *Infect. Immun.* **1987**, *55*, 472-476.

(17) Sperling, O.; Fuchs, A.; Lindhorst, T. K. Evaluation of the carbohydrate recognition domain of the bacterial adhesin FimH. Design, synthesis and binding properties of mannoside ligands. *Org. Biomol. Chem.* **2006**, *4*, 3913-3922.

(18) Han, Z.; Pinkner, J. S.; Ford, B.; Obermann, R.; Nolan, W.; Wildman, S. A.; Hobbs, D.; Ellenberger, T.; Cusumano, C. K.; Hultgren, S. J.; Janetka, J. W. Structure-based

drug design and optimization of mannoside bacterial FimH antagonists. *J. Med. Chem.* **2010**, *53*, 4779-4792.

(19) Klein, T.; Abgottspon, D.; Wittwer, M.; Rabbani, S.; Herold, J.; Jiang, X.; Kleeb, S.; Lüthi, C.; Scharenberg, M.; Bezençon, J.; Gubler, E.; Pang, L.; Smiesko, M.; Cutting, B.; Schwardt, O.; Ernst, B. FimH antagonists for the oral treatment of urinary tract infections: from design and synthesis to in vitro and in vivo evaluation. *J. Med. Chem.* **2010**, *53*, 8627-8641.

(20) Cusumano, C. K.; Pinkner, J. S.; Han, Z.; Greene, S. E.; Ford, B. A.; Crowley, J. R.; Henderson, J. P.; Janetka, J. W.; Hultgren, S. J. Treatment and prevention of urinary tract infection with orally active FimH inhibitors. *Sci. Transl. Med.* **2011**, *3*, 109ra115.

(21) Han, Z.; Pinkner, J. S.; Ford, B.; Chorell, E.; Crowley, J. M.; Cusumano, C. K.; Campbell, S.; Henderson, J. P.; Hultgren, S. J.; Janetka, J. W. Lead optimization studies on FimH antagonists: discovery of potent and orally bioavailable *ortho*-substituted biphenyl mannosides. *J. Med. Chem.* **2012**, *55*, 3945-3959.

(22) Pang, L.; Kleeb, S.; Lemme, K.; Rabbani, S.; Scharenberg, M.; Zalewski, A.; Schädler, F.; Schwardt, O.; Ernst, B. FimH antagonists: structure-activity and structure-property relationships for biphenyl α-D-mannopyranosides. *ChemMedChem.* **2012**, *7*, 1404-1422.

(23) Jiang, X.; Abgottspon, D.; Kleeb, S.; Rabbani, S.; Scharenberg, M.; Wittwer, M.; Haug, M.; Schwardt, O.; Ernst, B. Anti-adhesion therapy for urinary tract infections – a balanced PK/PD profile proved to be key for success. *J. Med. Chem.* **2012**, *55*, 4700-4713.

(24) Schwardt, O.; Rabbani, S.; Hartmann, M.; Abgottspon, D.; Wittwer, M.; Kleeb, S.; Zalewski, A.; Smiesko, M.; Cutting, B.; Ernst, B. Design, synthesis and biological

evaluation of mannosyl triazoles as FimH antagonists. *Bioorg. Med. Chem.* **2011**, *19*, 6454-6473.

(25) Brument, S.; Sivignon, A.; Dumych, T. I.; Moreau, N.; Roos, G.; Guérardel, Y.; Chalopin, T.; Deniaud, D.; Bilyy, R. O.; Darfeuille-Michaud, A.; Bouckaert, J.; Gouin, S. G. Thiazolylaminomannosides as potent antiadhesives of type 1 piliated *Escherichia coli* isolated from Crohn's disease patients. *J. Med. Chem.* **2013**, *56*, 5395-5406.

(26) Lindhorst, T. K.; Kieburg, C.; Krallmann-Wenzel, U. Inhibition of the type 1 fimbriae-mediated adhesion of *Escherichia coli* to erythrocytes by multiantennary D-mannosyl clusters: The effect of multivalency. *Glycoconj. J.* **1998**, *15*, 605-613.

(27) Nagahori, N.; Lee, R. T.; Nishimura, S.-L.; Pagé, S.; Roy, R.; Lee, Y. C. Inhibition of adhesion of type 1 fimbriated *Escherichia coli* to highly mannosylated ligands. *ChemBioChem* **2002**, *3*, 836-844.

(28) Appeldoorn, C. C. M.; Joosten, J. A. F.; Maate, F. A.; Dobrindt, U.; Hacker, J.; Liskamp, R. M. J.; Khan, A. S.; Pieters, R. J. Novel multivalent mannose compounds and their inhibition of the adhesion of type 1 fimbriated uropathogenic *E. coli*. *Tetrahedron Asym.* **2005**, *16*, 361-372.

(29) Patel, A.; Lindhorst, T. K. A modular approach for the synthesis of oligosaccharide mimetics. *Carbohydr. Res.* **2006**, *341*, 1657-1668.

(30) Touaibia, M.; Wellens, A.; Shiao, T. C.; Wang, Q.; Sirois, S.; Bouckaert, J.; Roy, R. Mannosylated G(0) dendrimers with nanomolar affinities to *Escherichia coli* FimH. *ChemMedChem* **2007**, *2*, 1190-1201.

(31) Durka, M.; Buffet, K.; Iehl, J.; Holler, M.; Nierengarten, J.-F.; Taganna, J.; Bouckaert, J.; Vincent, S. P. The functional valency of dodecamannosylated fullerenes with

Escherichia coli FimH - towards novel bacterial antiadhesives. *Chem. Commun.* **2011**, *47*, 1321-1323.

(32) Bouckaert, J.; Li, Z.; Xavier, C.; Almant, M.; Caveliers, V.; Lahoutte, T.; Weeks, S. D.; Kovensky, J.; Gouin, S. G. Heptyl α-D-mannosides grafted on a β-cyclodextrin core to interfere with *Escherichia coli* adhesion: An *in vivo* multivalent effect. *Chem. Eur. J.* **2013**, *19*, 7847-7855.

(33) Scharenberg, M.; Schwardt, O.; Rabbani, S.; Ernst, B. Target selectivity of FimH antagonists. *J. Med. Chem.* **2012**, *55*, 9810-9816.

(34) Choudhury, D.; Thompson, A.; Stojanoff, V.; Langermann, S.; Pinkner, J.; Hultgren, S. J.; Knight, S. D. X-ray structure of the FimC-FimH chaperone-adhesin complex from uropathogenic *Escherichia coli*. *Science* **1999**, *285*, 1061-1066.

(35) Hung, C.-S.; Bouckaert, J.; Hung, D.; Pinkner, J.; Widberg, C.; DeFusco, A.; Auguste, C. G.; Strouse, R.; Langermann, S.; Waksman, G.; Hultgren, S. J. Structural basis of tropism of *Eschrichia coli* to the bladder drug in urinary tract infection. *Mol. Microbiol.* **2002**, *44*, 903-915.

(36) Wellens, A.; Garofalo, C.; Nguyen, H.; Van Gerven, N.; Slättegard, R.; Henalsteens, J.-P.; Wyns, L.; Oscarson, S.; De Greve, H.; Hultgren, S. J.; Bouckaert, J. Intervening with urinary tract infections using anti-adhesives based on the crystal structure of the FimH-oligomannose-3 complex. *PLoS One* **2008**, *3*, e2040.

(37) Wellens, A.; Lahmann, M.; Touaibia, M.; Vaucher, J.; Oscarson, S.; Roy, R.; Remaut, H.; Bouckaert, J. The tyrosine gate as a potential entropic lever in the receptor-binding site of the bacterial adhesin FimH. *Biochemistry* **2012**, *51*, 4790-4799.

(38) Totsika, M.; Kostakioti, M.; Hannan, T. J.; Upton, M.; Beatson, S. A.; Janetka, J. W.; Hultgren, S. J.; Schembri, M. A. A FimH inhibitor prevents acute bladder infection and

treats chronic cystitis caused by multidrug-resistant uropathogenic *Escherichia coli* ST131. *J. Infect. Dis.* **2013**, *208*, 921-928.

(39) Meanwell, M. A. Synopsis of some recent tactical application of bioisosteres in drug design. *J. Med. Chem.* **2011**, *54*, 2529-2591.

(40) Prieto, M.; Zurita, E.; Rosa, E.; Luñoz, L.; Lloyd-Williams, P.; Giralt, E. Arylboronic acids and arylpinacolboronate esters in Suzuki coupling reactions involving indoles. Partner role swapping and heterocycle protection. *J. Org. Chem.* **2004**, *69*, 6812-6820.

(41) Schulz, M. J.; Coats, S. J.; Hlasta, D. J. Microwave-assisted preparation of aryltetrazoleboronate esters. *Org. Lett.* **2004**, *6*, 3265-3268.

(42) Devos, A.; Remion, J.; Frisque-Hesbain, A. M.; Colens, A.; Ghosez, L. Synthesis of acyl halides under very mild conditions. *J. Chem. Soc. Chem. Commun.* **1979**, 1180-1181.

(43) Rabbani, S.; Jiang, X.; Schwardt, O.; Ernst, B. Expression of the carbohydrate recognition domain of FimH and development of a competitive binding assay. *Anal. Biochem.* **2010**, *407*, 188-195.

(44) Waetherman, R.V.; Kiessling, L.L. Fluorescence anisotropy assay reveals affinities of *C*- and *O*-glycosides for concanavalin A. *J. Org. Chem.* **1996**, *61*, 534-538.

(45) Cer, R. Z.; Mudunuri, U.; Stephens, R.; Lebeda, F. J. IC50-to-Ki: a web-based tool for converting IC50 to Ki values for inhibitors of enzyme activity and ligand binding. *Nucleic Acids Research*, **2009**, *37*, W441-W445.

(46) Lynch, B. A.; Loiacono, K. A.; Tiong, C. L.; Adams, S. E.; MacNeil, I. A. A Fluorescence Polarization Based Src-SH2 Binding Assay. *Anal. Biochem.* **1997**, 247, 77-82.

(47) Wu, P.; Brasseur, M.; Schindler, U. A High-Throughput STAT Binding Assay Using Fluorescence Polarization *Anal. Biochem*. **1997**, 249, 29-36.

(48) Huang, X. Fluorescence Polarization Competition Assay: The Range of Resolvable Inhibitor Potency Is Limited by the Affinity of the Fluorescent Ligand *J. Biomol. Screen.* **2003**, 8, 34-38.

(49) Cooper, A. *Biophysical Chemistry, 2nd Edition.* RSC Publishing. Cambridge UK. **2011**, pp. 122-123.

(50) Scharenberg, M.; Jiang, X.; Pang, L.; Navarra, G.; Rabbani, S.; Binder, F.; Schwardt, O.; Ernst, B. Kinetic properties of carbohydrate-lectin interactions: FimH antagonists. *ChemMedChem* **2014**, *9*, 78-83.

(51) Cabani, S.; Gianni, P.; Mollica, V.; Lepori, L. Group contribution to the thermodynamic properties of non-ionic solutes in dilute aqueous solution. *J. Solution Chem.* **1981**, *10*, 563-595.

(52) Hansch, C.; Leo, A.; Taft, R.W. A survey of Hammett substituent constants and resonance and field parameters. *Chem. Rev.* **1991**, *91*, 165-195.

(53) Chen, A.; Wadso, I. Simultaneous determination of delta G, delta H and delta S by an automatic microcalorimetric titration technique: application to protein ligand binding. *J Biochem Biophys Meth,* **1982**, *6*, 307-316.

(54) Freire, E.; Mayorga, O.L.; Straume, M. Isothermal titration calorimetry. *Anal Chem*, **1990**, *62*, 950A-959A.

(55) Wiseman, T.; Williston, S.; Brandts, J. F.; Lin, L.-N. Rapid measurement of binding constants and heats of binding using a new titration calorimeter. *Anal. Biochem.* **1989**, *179*, 131-137.

(56) Turnbull, W. B.; Daranas A.H. On the value of c: can low affinity systems be studied by isothermal titration calorimetry? *J. Am. Chem. Soc.* **2003**, *125*, 14859-14866.

(57) Sigurskjold B. W. Exact analysis of competition ligand binding by displacement isothermal titration calorimetry. *Anal. Biochem.* **2000**, *277*, 260-266.

(58) Velazquez-Campoy A.; Freire E. Isothermal titration calorimetry to determine association constants for high-affinity ligands. *Nat. Protoc.* **2006**, *1*, 186-191.

(59) Dearden, J. C.; Bresnen, G. M. The measurement of partition coefficients. *QSAR Comb. Sci.* **1988**, *7*, 133-144.

(60) Kansy, M.; Senner, F.; Gubernator, K. Physicochemical high throughput screening: parallel artificial membrane permeation assay in the description of passive absorption processes. *J. Med. Chem.* **1998**, *41*, 1007-1010.

(61) Hubatsch, I.; Ragnarsson, E. G. E.; Artursson, P. Determination of drug permeability and predicition of drug absorption in Caco-2 monolayers. *Nat. Protoc.* **2007**, *2*, 2111-2119.

(62) Banker, M. J.; Clark, T. H.; Williams, J. A. Development and validation of a 96-well equilibrium dialysis apparatus for measuring plasma protein binding. *J. Pharm. Sci.* **2003**, *92*, 967-974.

(63) Obach, R. S. Prediction of human clearance of twenty-nine drugs from hepatic microsomal intrinsic clearance data: an examination of in vitro half-life approach and nonspecific binding to microsomes. *Drug Metab. Dispos.* **1999**, *27*, 1350-1359.

(64) Chaturvedi, P. R.; Decker, C. J.; Odinecs, A. Prediction of pharmacokinetic properties using experimental approaches during early drug discovery. *Curr. Opin. Chem. Biol.* **2001**, *5*, 452-463.

(65) Di, L.; Kerns, E. H. Profiling drug-like properties in discovery research. *Curr. Opin. Chem. Biol.* **2003**, *7*, 402-408.

(66) Lipinski, C. A. Drug-like properties and the causes of poor solubility and poor permeability. *J. Pharmacol. Toxicol. Methods* **2000**, *44*, 235-249.

(67) Curatolo, W. Physical chemical properties of oral drug candidates in the discovery and exploratory development settings. *Pharm. Sci. Techn. Today* **1998**, *1*, 387-393.

(68) Ishikawa, M.; Hashimoto, Y. Improvement in aqueous solubility in small molecule drug discovery programs by disruption of molecular planarity and symmetry. *J. Med. Chem.* **2011**, *54*, 1539-1554.

(69) Avdeef, A.; Bendels, S.; Di, L.; Faller, B.; Kansy, M.; Sugano, K.; Yamauchi, Y. PAMPA – critical factors for better predictions of absorption. *J. Pharm. Sci.* **2007**, *96*, 2893-2909.

(70) Artursson, P.; Karlsson, J. Correlation between oral drug absorption in humans and apparent drug permeability coefficients in human intestinal epithelial (Caco-2) cells. *Biochem. Biophys. Res. Commun.* **1991**, *175*, 880-885.

(71) Feng, B.; LaPerle, J. L.; Chang, G.; Varma, M. V. S. Renal clearance in drug discovery and development: molecular descriptors, drug transporters and disease state. *Expert Opin. Drug. Metab. Toxicol.* **2010**, *6*, 939-952.

(72) Schmidt, S.; Gonzalez, D.; Derendorf, H. Significance of protein binding in pharmacokinetics and pharmacodynamics. *J. Pharm. Sci.* **2010**, *99*, 1107-1122.

(73) Weisiger, R. A. Dissociation from albumin: A potentially rate-limiting step in the clearance of substances by the liver. *Proc. Natl. Acad. Sci. USA* **1985**, *82*, 1563-1567.

(74) Smith, D. A.; Jones, B. C.; Walker, D. K. Design of drugs involving the concepts and theories of drug metabolism and pharmacokinetics. *Med. Res. Rev.* **1996**, *16*, 243-266.

(75) Van de Waterbeemd, H.; Smith, D. A.; Beaumont, K.; Walker, D. K. Property-based design: optimization of drug absorption and pharmacokinetics. *J. Med. Chem.* **2001**, *44*, 1313-1333.

(76) Varma, M. V. S.; Feng, B.; Obach, R. S.; Troutman, M. D.; Chupka, J.; Miller, H. R.; El-Kattan, A. Physicochemical determinants of human renal clearance. *J. Med. Chem.* **2009**, *52*, 4844-4852.

(77) Waring, M. J. Lipophilicity in drug discovery. *Expert Opin. Drug Discov.* **2010**, *5*, 235-248.

(78) Zhang Y.; Huo M.; Solver, P.K. An Add-in program for pharmacokinetic and pharmacodynamic data analysis in Microsoft Excel, *Computer Methods and Programs in Biomedicine* **2010**, *99*, 306-314.

(79) Scharenberg, M.; Abgottspon, D.; Cicek, E.; Jiang, X.; Schwardt, O.; Rabbani, S.; Ernst, B. Cytometry-Based Assay for Screening FimH Antagonists. *Assay and Drug Development Technologies* **2011**, *9*, 455-464.

(80) Hooton, T. M. Fluoroquinolones and resistance in the treatment of uncomplicated urinary tract infection. *Int. J. Antimicrob. Agents* **2003**, *22*, 65-72.

(81) Jakobsen, L.; Cattoir V.; Jensen, K. S.; Hammerum, A. M.; Nordmann, P.; Frimodt-Møller N. Impact of low-level fluoroquinolone resistance genes qnrA1, qnrB19, and qnrS1 on ciprofloxacin treatment of isogenic *Escherichia coli* strains in a murine urinary tract infection model. *J Antimicrob. Chemother.* **2012**, *67*, 2438-2444.

(82) Mulvey, M. A. Adhesion and entry of uropathogenic *Escherichia coli*. *Cell Microbiol.* **2002**, *4*, 257– 271.

(83) Ballatore, C.; Huryn, D. M.; Smith, A. B. Carboxylic acid (bio)isosteres in drug design. *ChemMedChem* **2013**, *8*, 385-395.

(84) Justice, S. S.; Hung, C.; Theriot, J. A.; Fletcher, D. A.; Anderson, G. G.; Footer, M. J.; Hultgren, S. J. Differentiation and developmental pathways of uropathogenic Escherichia coli in urinary tract pathogenesis. *Proc Natl Acad Sci U S A.* **2004**, *101*, 1333–8.

(85) Mulvey, M. A.; Schilling, J.D.; Hultgren, S. J. Establishment of a Persistent Escherichia coli Reservoir during the Acute Phase of a Bladder Infection. *Infect. Immun*. **2001**, *69*, 4572–9.

(86) Houtman, J. C.; Brown, P. C.; Bowden, B.; Yamaguchi, H.; Appella, E.; Samelson, L. E.; Schuck, P. Studying multisite binary and ternary protein interactions by global analysis of isothermal titration calorimetry data in SEDPHAT: application to adaptor protein complexes in cell signaling. *Protein Sci.* **2007**, *16*, 30-42.

(87) Maestro, version 9.3, Schrödinger, LLC, New York, NY, 2012.

(88) MacroModel, version 9.9, Schrödinger, LLC, New York, NY, 2012.

(89) AMSOL, version 7.1, Hawkins, G. D.; Giesen, D. J.; Lynch, G. C.; Chambers, C. C.; Rossi, I.; Storer, J. W.; Li, J.; Thompson, J. D.; Winget, P.; Lynch, B. J.; Rinaldi, D.; Liotard, D. A.; Cramer, C. J.; Truhlar, D. G. University of Minnesota, Minneapolis, 2003; based in part on AMPAC, version 2.1, Liotard, D. A.; Healy, E. F.; Ruiz, J. M.; Dewar, M. J. S.

(89) Chambers, C. C.; Hawkins, G. D.; Cramer, C. J.; Truhlar, D. G. Model for aqueous solvation based on class IV atomic charges and first solvation shell effects. *J. Phys. Chem.* **1996**, *100*, 16385-16398.

(91) Dewar, M. J. S.; Zoebisch, E. G.; Healy, E. F.; Stewart, J. J. P. AM1 - A new general-purpose quantum-mechanical molecular-model (Vol. 107, PG 3902, 1985). *J. Am. Chem. Soc.* **1993**, *115*, 5348-5348.

(92) Mulvey, M. A.; Schilling, J. D.; Hultgren, S. J. Establishment of a persistent *Escherichia coli* reservoir during the acute phase of a bladder infection. *Infect. Immun.* **2001**, *69*, 4572-4579.

(93) Kabsch, W. Automatic Processing of Rotation Diffraction Data from Crystals of Initially Unknown Symmetry and Cell Constants. *J. Appl. Crystallogr.* **1993**, *26*, 795-800.

(94) Leslie, A. G. W. The integration of macromolecular diffraction data. *Acta Crystallogr. D* **2006**, *62*, 48-57.

(95) Winn, M. D.; Ballard, C. C.; Cowtan, K. D.; Dodson, E. J.; Emsley, P.; Evans, P. R.; Keegan, R. M.; Krissinel, E. B.; Leslie, A. G. W.; McCoy, A.; McNicholas, S. J.; Murshudov, G. N.; Pannu, N. S.; Potterton, E. A.; Powell, H. R.; Read, R. J.; Vagin, A.; Wilson, K. S. Overview of the CCP4 suite and current developments. *Acta Crystallogr. D* **2011**, *67*, 235-242.

(96) McCoy, A. J. Solving structures of protein complexes by molecular replacement with Phaser. *Acta Crystallogr. D* **2007**, *63*, 32-41.

(97) Emsley, P.; Cowtan, K. Coot: model-building tools for molecular graphics. *Acta Crystallogr D* **2004**, *60*, 2126-2132.

(98) Adams, P. D.; Grosse-Kunstleve, R. W.; Hung, L.-W.; Ioerger, T. R.; McCoy, A. J.;Moriarty, N. W.; Read, R. J.; Sacchettini, J. C.; Sauter, N. K.; Terwilliger, T. C. PHENIX: building new software for automated crystallographic structure determination. *Acta Crystallogr. D Biol. Crystallogr.* **2002**, *58*, 1948–1954.

(99) van Aalten, D. M. F.; Bywater, R.; Findlay, J. B. C.; Hendlich, M.; Hooft, R. W. W.; Vriend, G. PRODRG, a program for generating molecular topologies and unique

molecular descriptors from coordinates of small molecules. *J. Comput. Aided Mol. Des.* **1996**, *10*, 255-262.

(100) Chen, V. B.; Arendall, W. B.; Headd, J. J.; Keedy, D. A.; Immormino, R. M.; Kapral, G. J.; Murray, L. W.; Richardson, J. S.; Richardson, D. C. MolProbity: all-atom structure validation for macromolecular crystallography. *Acta Crystallogr*. *D* **2010,** *66*, 12-21.

(101) Bezençon, J.; Wittwer, M. B.; Cutting, B.; Smiesko, M.; Wagner, B.; Kansy, M.; Ernst, B. pK_a determination by ^{1}H NMR spectroscopy – an old methodology revisited. *J. Pharm. Biomed. Anal.* **2014**, *93*, 147-155.

(102) (a) VCCLAB, Virtual Computational Chemistry Laboratory, 2005, http://www.vcclab.org (accessed August 14, 2012); (b) Tetko, I. V.; Gasteiger, J.; Todeschini, R.; Mauri, A.; Livingstone, D.; Ertl, P.; Palyulin V. A.; Radchenko, E. V.; Zefirov, N. S.; Makarenko, A. S.; Tanchuk, V. Y.; Prokopenko, V. V. Virtual computational chemistry laboratory – design and description. *J. Comput. Aided Mol. Des.* **2005**, *19*, 453-463.

(103) Diehl K-H.; Hull R. A. Good Practice Guide to the Administration of Substances and Removal of Blood, Including Routes and Volumes. *J. Appl. Toxicol.* **2001**, *21*, 15-23.

Table of Content graphic

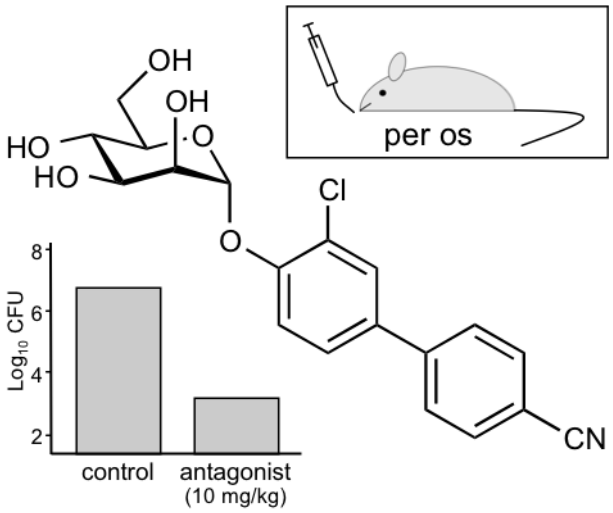

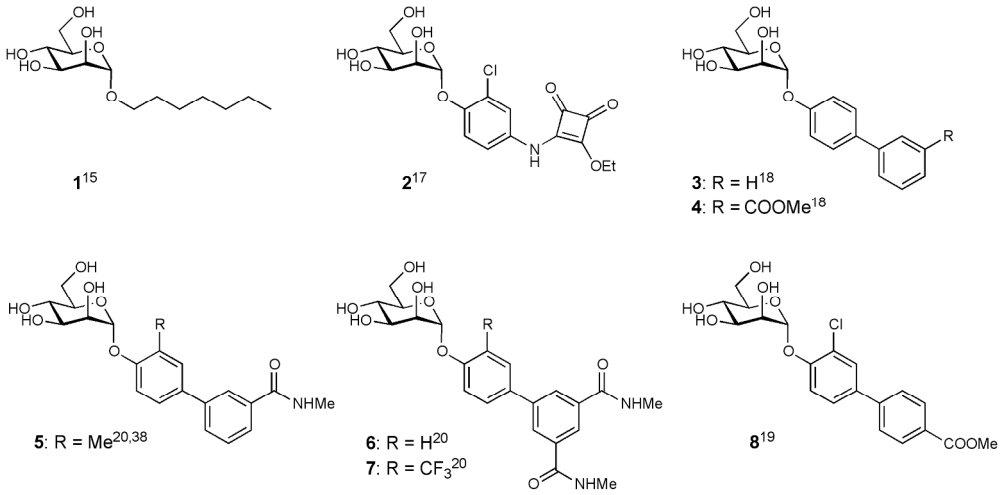

Figure 1. Monovalent FimH antagonists 1-4 acting as reference compounds and 5-8 which have been orally explored in in vivo disease models.
213x104mm (300 x 300 DPI)

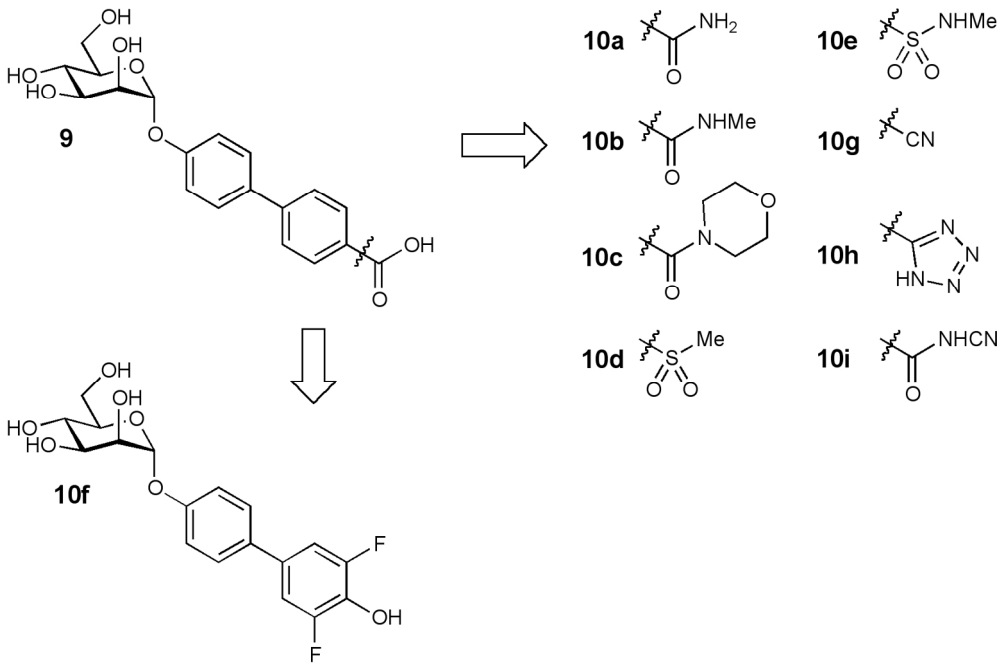

Figure 2. Bioisosteric replacement of the carboxylic acid substituent of biphenyl α-D-mannopyranoside 9.
152x101mm (300 x 300 DPI)

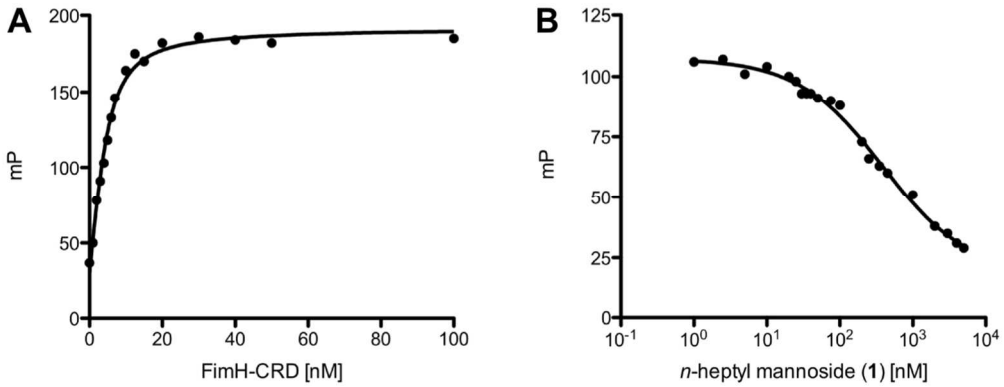

Figure 3. A) Direct binding curve of the labeled competitor 23 obtained by adding a linear dilution of FimH-CRD (0-100 nM) and a constant concentration of competitor 23 (5 nM). The KD was determined by fitting the experimental data to a single-site binding fit that accounts for ligand depletion. In three FP based direct binding experiments the KD of competitor 23 was determined to be 1.7 nM. B) Inhibition curve of n-heptyl mannoside (1) from the competitive FP assay. The IC50 value was determined by nonlinear least-squares fitting to a standard 4-parameter equation. A modified Cheng-Prusoff equation45 was used to calculate the corresponding KD value (KD = 28.3 nM).
209x80mm (150 x 150 DPI)

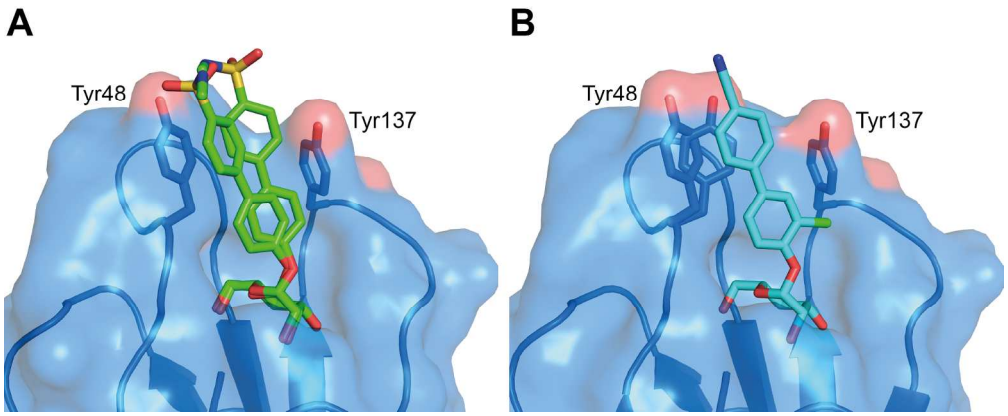

Figure 4. Ligand binding poses determined by X-ray co-crystallization with compounds 10e resolved to 1.07 Å (A) and 10j resolved to 1.10 Å (B). The electron density surrounding the aglycone of 10e indicates flexibility of the aglycone and was modeled in two poses. Both compounds bind in a similar pose with a well-defined hydrogen network surrounding the mannose moiety and π-π stacking interactions between the second aromatic ring and Tyr48 side-chain (A). In contrast, in the FimH-CRD/10j structure the amino acid side chain of Y48 can be modeled in two distinct rotamers, suggesting flexibility also of the receptor (B).
189x78mm (300 x 300 DPI)

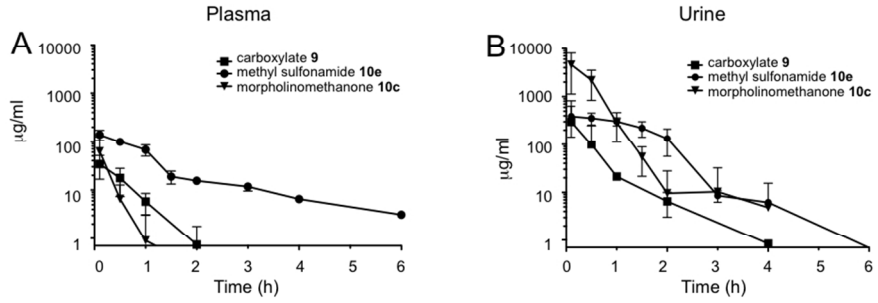

Figure 5. Antagonist concentrations in (A) plasma and (B) urine after a single iv application of 9, 10c, and 10e (50 mg/kg).
180x67mm (150 x 150 DPI)

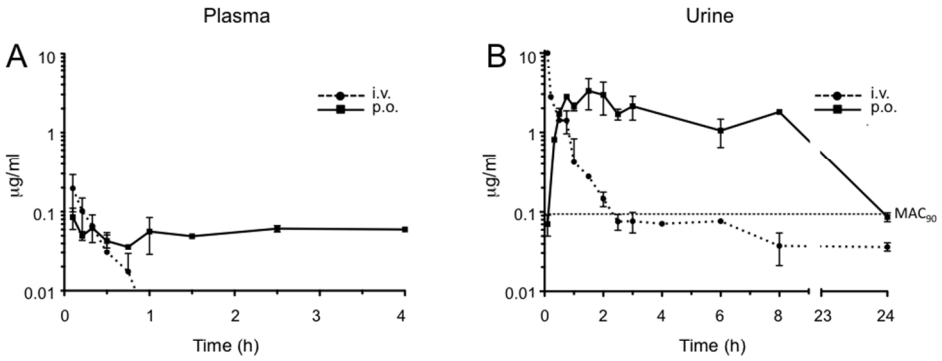

Figure 6. Antagonist concentrations in (A) plasma and (B) urine after a single iv and po application of compound 10j (iv: 0.625 mg/kg; po: 1.25 mg/kg). MAC90, minimal anti-adhesive concentration to inhibit 90% adhesion (0.094 µg/mL).
175x79mm (150 x 150 DPI)

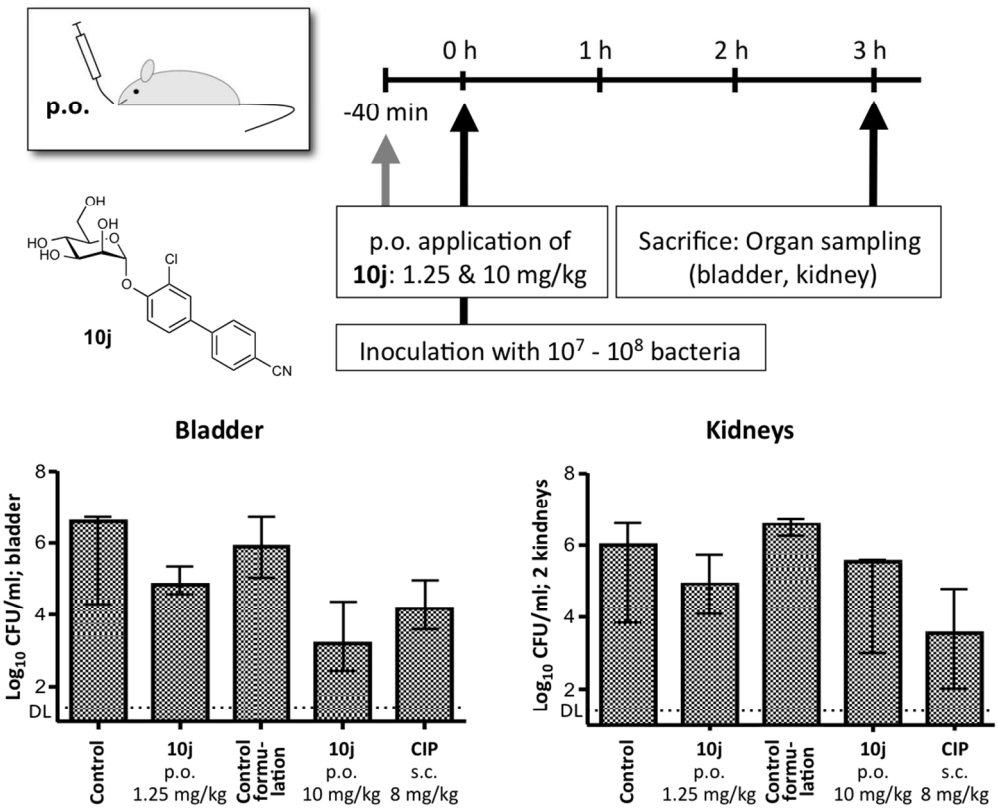

Figure 7. Preventive efficacy of 10j in the UTI mouse model 3 h after infection. The bars depict the median bacterial load with the interquartile range in the different study groups. Shown are the results of the control group (PBS), control group formulation (5% DMSO in PBS containing 1% Tween 80), and the intervention groups with the preventive applications of either, 1.25 mg/kg or 10 mg/kg 10j p.o. or 8 mg/kg CIP s.c. (representing the murine dose equivalent to a human standard dose).81 DL, detection limit; CFU, colony forming units.
205x165mm (150 x 150 DPI)

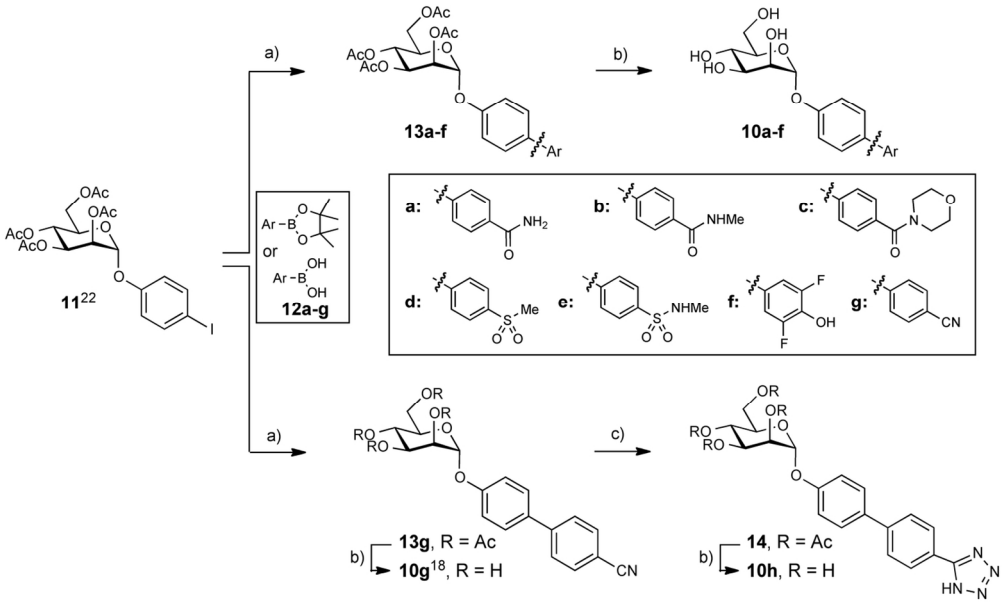

Scheme 1. a) Pd(Cl2)dppf·CH2Cl2, K3PO4, DMF, 80 °C, 4 h (13a-g, 44-99%); b) NaOMe, MeOH, rt, 4 h (10a-h, 29-86%); c) TMSN3, Bu2Sn(O), DME, 150 °C, μW, 10 min (81%).
127x76mm (300 x 300 DPI)

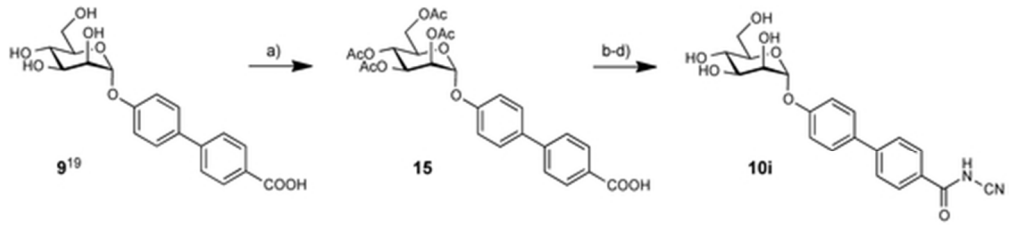

Scheme 2. a) i) Ac2O, DMAP, pyridine, 0 °C to rt, overnight; ii) satd. NaHCO3 aq., DCM, rt, 2 h (15, 53%); b) 1-chloro-N,N,2-trimethyl-1-propenylamine, toluene, 0 °C to rt, 2 h; c) NaH, NH2CN, DMF, 0 °C to rt, overnight; d) NaOMe, MeOH, rt, 4 h (10i, 21% for three steps).
48x10mm (300 x 300 DPI)

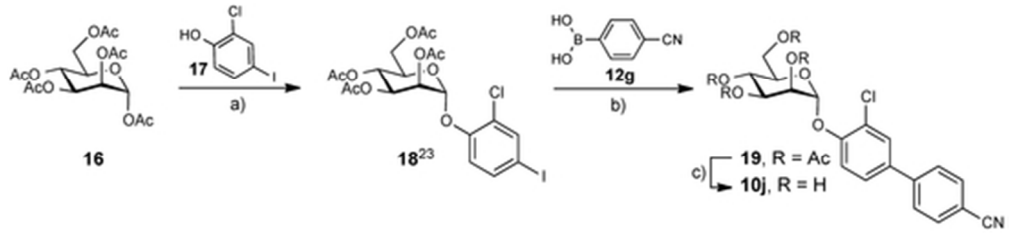

Scheme 3. a) BF3·Et2O, CH2Cl2, 40 °C (76%); b) Pd(Cl2)dppf·CH2Cl2, K3PO4, DMF, 80 °C (75%); c) NaOMe, MeOH, rt, 4 h (48%).
46x10mm (300 x 300 DPI)

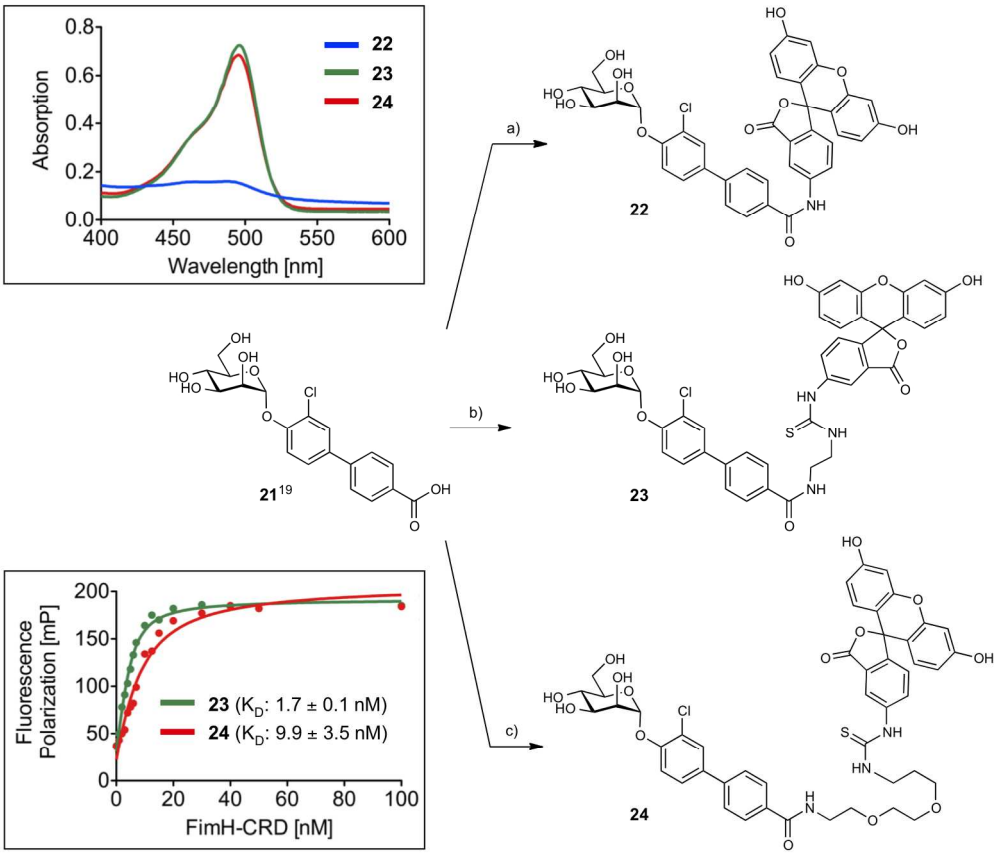

Scheme 4. a) 1-[(1-(Cyano-2-ethoxy-2-oxoethylideneaminooxy)-dimethylamino-morpholinomethylene)] methanaminium hexafluorophosphate (COMU), NEt3, fluoresceinamine, DMF, rt, 7 h (22, 19%); b) i. DIC, NHS, N-Boc-ethylenediamine, DMF, rt, 12 h; ii. TFA, DCM, rt, 10 min (68% over two steps), iii. fluorescein isothiocyanate (FITC), NEt3, DMF, rt, 3 h (23, 48%); c) i. DIC, NHS, N-Boc-PEG2-NH2, DMF, rt, 14 h; ii. TFA, DCM, rt, 30 min (62% over two steps); iii. FITC, DMF, rt (24, 65%).
185x158mm (300 x 300 DPI)

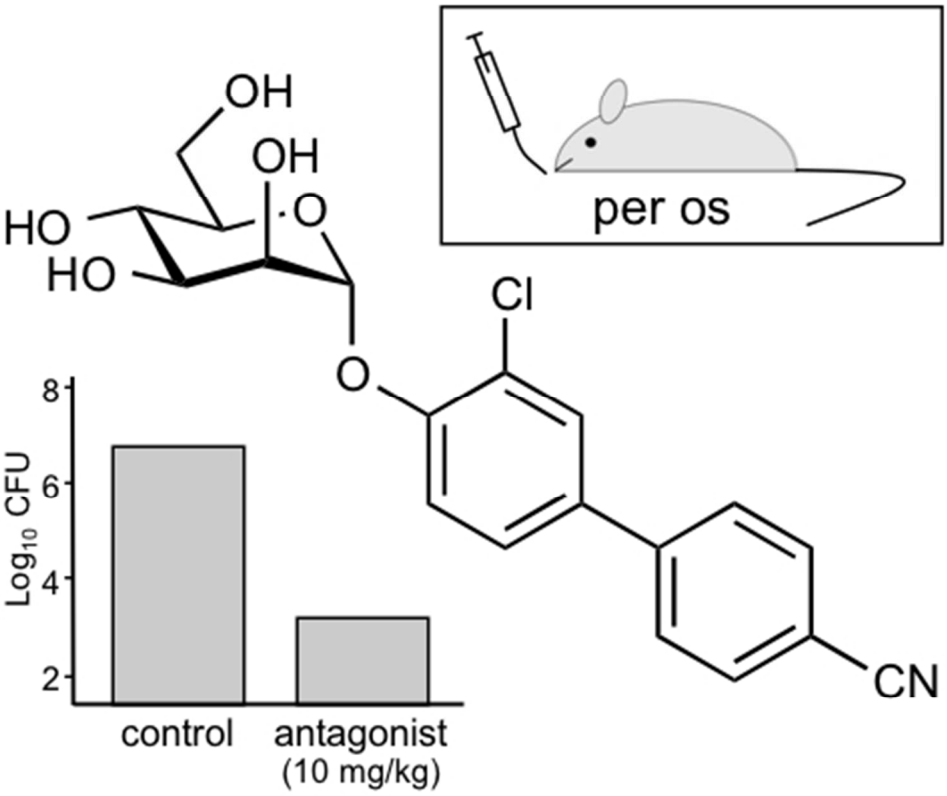

81x67mm (150 x 150 DPI)